CrystEngComm

Accepted Manuscript

ROYAL SOCIETY OF CHEMISTRY

www.rsc.org/crystengcomm

Shape-Controlled Iron Oxide Nanocrystals: Synthesis, Magnetic Properties and Energy Conversion Applications

J. Liu,[#] Z. Wu,[#] Q. Tian, W. Wu, and X. Xiao**

School of Physics and Technology and School of Printing and Packaging, Wuhan University, Wuhan 430072, P. R. China

[#] These authors contributed equally.

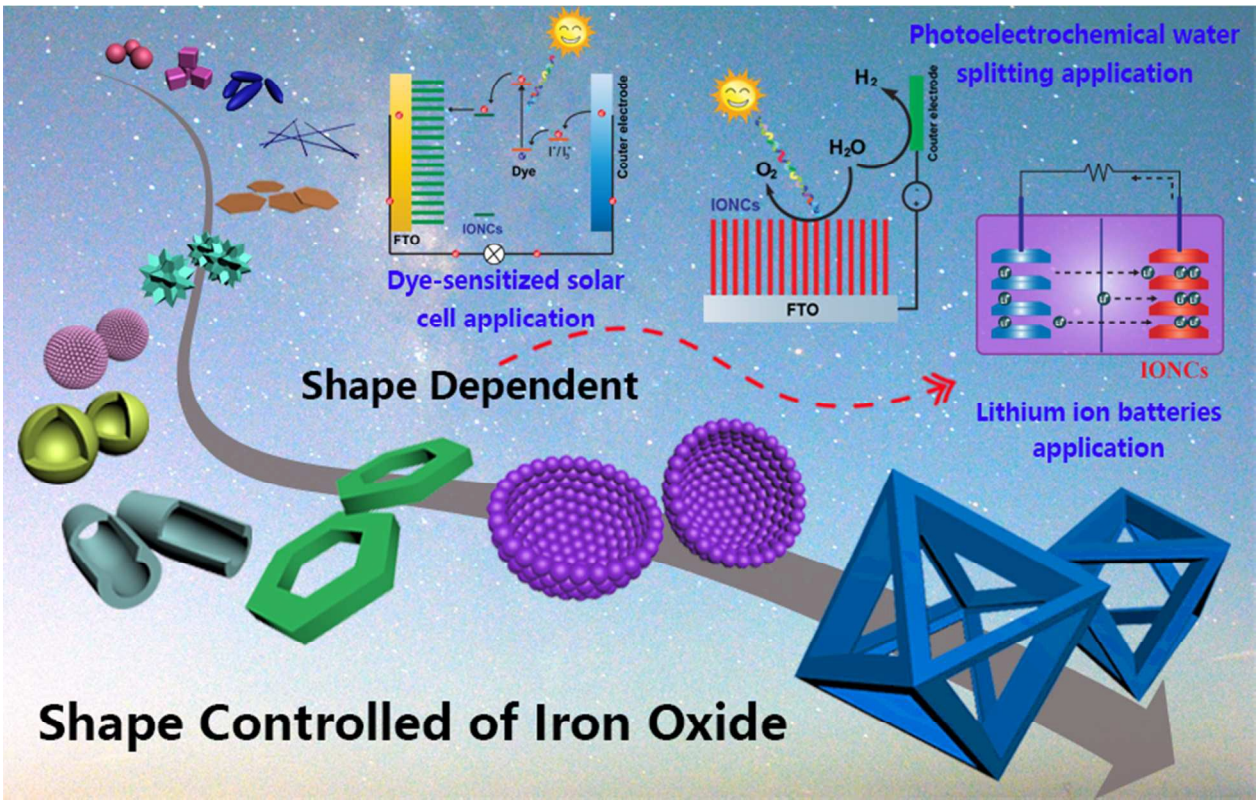

Shape-Controlled Iron Oxide Nanocrystals: Synthesis, Magnetic Properties and Energy Conversion Applications

*Jun Liu,[#1] Zhaohui Wu,[#1] Qingyong Tian[1], Wei Wu,[1,2] * and Xiangheng Xiao[1,2]**

[1]School of Physics and Technology and School of Printing and Packaging, Wuhan University, Wuhan 430072, P. R. China

[2]Suzhou Research Institute of Wuhan University, Suzhou 215000, P. R. China

[#] These authors contributed equally.

Abstract Iron oxide nanocrystals (IONCs) with various geometric morphologies show excellent physical and chemical properties and have received extensive attention in recent years. The various shapes of IONCs induced magnetic and electrochemical properties to endow the IONCs with diverse applications. Understanding the correlation between the physicochemical properties and morphology of IONCs is a prerequisite for their widespread applications. Hence, this review focus on current research progresses of the shape-controlled IONCs in different dimensions and the corresponding shape-dependent magnetic, catalytic and gas sensor properties are discussed. Furthermore, the general preparation methods, shape-guided growth mechanisms and energy conversion applications in photoelectrochemical water splitting, dye-sensitized solar cells (DSSCs) and lithium ion batteries (LIBs)

*To whom correspondence should be addressed. Tel: +86-27-68778529. Fax: +86-27-68778433. E-mail: weiwu@whu.edu.cn (W. Wu), xxh@whu.edu.cn (X.H. Xiao)

of these IONCs (α-Fe_2O_3, γ-Fe_2O_3, Fe_3O_4) are also discussed. Finally, the perspectives of IONCs in promising research directions are proposed.

Keywords: iron oxides; shape controlling; synthesis; mechanisms; magnetic property; energy conversion application

Contents

References

1 Introduction

Since 1984, German scientist Gleiter were successfully prepared Fe nanoparticles (NPs) *via* inert-gas condensation method,[1] the synthesis of metal Fe and corresponding iron oxide nanocrystals (IONCs) in nanoscale have attracted more attentions because of their unique response and flexible manipulability under magnetic fields, especially for the IONCs. The IONCs are mainly consist of magnetite (Fe_3O_4), hematite (α-Fe_2O_3), β-Fe_2O_3, maghemite (γ-Fe_2O_3), ε-Fe_2O_3 and wustite iron (FeO). These IONCs with different crystal structures providing desirable properties are frequently used in biomedicine, energy, and industry.[2-9] However, the effects of size and morphology on the properties of IONCs still draw a little of attentions.

Recently, the morphological diversification of IONCs and their shape-dependent properties are well noticed for diverse applications. From the morphologies aspect, the IONCs are classified into solid, mesoporous and hollow IONCs. As shown in **Figure 1, Figure 4** and **Figure 6,** the solid IONCs include 0D nanospheres/nanopolyhedrons, 1D nanorods/nanowires/nanoshuttles, 2D disks and 3D nanoflowers/namostars/nanourchins. The mesoporous IONCs are 0D mesoporous nanospheres/nanocubes and 1D mesoporous nanorods/nanoshuttles. The hollow IONCs are relatively novel structures, which include 0D hollow nanospheres/nanopolyhedrons, 1D hollow nanotubes/nanowires/nanodumbbells, 2D nanorings and 3D nanoframes/nanobowl/hollow multiple nanospheres, *etc*. For synthesis of the solid IONCs with desirable morphology, a number of methods are developed. Generally, traditional co-precipitation method is used for synthesis of spherical 0D IONCs, hydrothermal and thermal decomposition methods are always tended to prepare IONCs with tunable shapes ranging from 0D nanopolyhedrons to 1D nanorods/shuttles. Moreover, hydrothermal method is also the most common approach for synthesis of 2D and 3D IONCs because of the easily controlling process under high temperature and pressure. Template method, hydrothermal method and high-

temperature calcination method are considered as the favor routes to realize the mesoporous or hollow structures of IONCs.

The as-synthesized IONCs with diversified morphologies showed the tunable novel performances, such as shape-dependent surface free energy, catalytic/sensing activities and magnetic property. It is well known that the different exposed facets of nanocrystals (NCs) are shown because of the shape change, then, the properties of NCs are developed for desirable applications because of their surface energy and chemical activities. For example, α-Fe_2O_3 NCs with three kinds of morphologies (bipyramid, pseudocube and plate) are synthesized with exposure of {113}, {012} or {001} facets, respectively. These α-Fe_2O_3 NCs exhibit much different gas sensing properties, and these properties are directly proportional to the surface energies of these α-Fe_2O_3 NCs ({113} > {012} > {001}). The oxygen-chemisorbed ability of those facets is different because of the variation in the atomic configurations and chemical composition on di□erent facets.[10] Rhombic dodecahedral Fe_3O_4 NCs with exposed high-energy {110} facet show excellent peroxidase-like activity by comparing with spherical Fe_3O_4 and commercial Fe_3O_4 NPs.[11] Additionally, most of IONCs are the magnetic materials, which can be manipulated by an external magnetic field.[12, 13] The lowest energy state of a magnetic particle depends on its size, shape and anisotropic character, and the magnetic properties of IONCs are especially influenced by their shapes in many ways.[14] For example, Wang and co-workers prepared α-Fe_2O_3 nanorods and nanotubes, and investigated their shape-dependent magnetic performance. The results reveal that the magnetic property is strongly depending on their shape. Morin transition at 166 K from canted antiferromagnetic state to antiferromagnetic state could be found in nanorods, but the nanotubes exhibit a 3D magnetic ordering above 300 K, which are attributed to the small particles in a few regions of the tubes.[15]

The shape-dependent properties facilitate these IONCs to be applied in various fields. For example, ultrafine superparamagnetic Fe_3O_4 NPs without magnetic hysteresis are optimal choice in biomedicine application. However, the mesoporous/hollow IONCs with larger specific surface area are the preferential option for chemical gas reaction in sensor application.[16, 17] Furthermore, the shape-

dependent properties of IONCs could also be used for energy conversion application, in which these IONCs could act as medium for transferring one kind of energy to another. Different morphologies of IONCs possess different advantages in energy conversion application. Because a lot of properties could be affected by the shape of IONCs, such as specific surface area,[18, 19] chemical activity,[20] electroconductibility[21] and magnetic property.[15] In photoelectrochemical water splitting and DSSCs application, nanopolyhedrons IONCs with exposed high energy facets show the high chemical activities because of the kink atoms with low coordination number on these facets. On the other hand, IONCs with mesoporous/hollow structures of are also the favorable structures for catalysis, because the larger specific surface area of IONCs and they possess more "active-sites" in excitation of electrons.[22] In lithium ions battery (LIBs) application, the unique mesoporous/hollow structure of IONCs are preferred than other structures.[23] Specifically, the hollow structure of IONCs is facilitated for penetration of the electrolyte and transportation of Li^+ ions in the electrode. Moreover, hollow IONCs could also server as efficiently buffer of the stress caused by volume variation during the charge-discharge process.[24, 25]

Recently, alterable dimensional shapes and shape-dependent properties of IONCs have received more attentions. So far, however, few reviews are focus on these shape-controlled synthesis of IONCs comprehensively. Therefore, the systematical summary of shape-controlled synthesis and formation mechanisms of IONCs is particularly necessary. Comparing the properties of IONCs with different morphologies is also a research focus, and the shape-dependent energy conversion applications of IONCs still need to develop further. Therefore, the recent developments in classified characteristic and shape-dependent properties of IONCs with various morphologies (solid, mesoporous and hollow structure) are firstly present. Then, we briefly overview the preparation method of IONCs with various morphologies. Further investigates of proposed growth mechanisms for precisely shape controlling process of IONCs are also discussed. Finally, the shape-dependent energy conversion applications of these IONCs in photoelectrochemical water splitting, DSSCs and LIBs application are concluded and discussed.

2. Shape-controlled IONCs and shape-dependent properties of IONCs

2.1. Shape-controlled IONCs

2.1.1. Solid IONCs

Solid-structured IONCs represent a crucial class of materials among all different shapes of IONCs in the past decades. Herein, the classification of various shape of solid IONCs is introduced according to different dimension, including isotropic 0D spheres and polyhedrons, anisotropic 1D rods and wires, 2D discs and prisms, and 3D NCs, as illustrated in **Figure 1**.

0D spheres and polyhedrons. 0D spheres of IONCs are the most common shapes among all kind shapes of IONCs. Typically, 0D spherical IONCs present some superior properties, such as low surface free energy, high surface areas and superparamagnetism. Such properties of 0D IONCs prompt the widely applications in biomedicine and catalysis.[26, 27] In synthesis of 0D spherical IONCs, simple preparation methods and inexpensive raw materials are also the advantages to their applications. The common preparation routes for spherical IONCs are involved co-precipitation and thermal decomposition routes, which are well controlled during nucleation and growth processes.[28, 29] In co-precipitation, without any surfactants, the spherical IONCs are formed by homogeneous nucleation and isotropic growth. And final spherical NPs with low surface free energy is driven by the kinetic factor during the growth process. But the size distribution of these spherical IONCs is too broad, because of the broad-distributed of supersaturation for nucleation and only kinetic controlling for crystal growth.[30] Compared with co-precipitation, spherical IONCs synthesized by thermal decomposition route present more accurate spherical morphology, higher monodispersity, narrower size distribution and higher crystallinity. Because complex hydrolysis reactions appeared in co-precipitation method can be avoided in the thermal decomposition method, and the nucleation is separated from growth.[31, 32]

In terms of the polyhedral IONCs, which include tetrahedrons, cubes, octahedrons and dodecahedrons, *etc*. Compared with the spherical IONCs, these polyhedral IONCs possess a particular characteristic that a great number of high-energy facets are exposed. For example, the cubic α-Fe_2O_3 NCs with exposed {104} facets and rhombic dodecahedral Fe_3O_4 NCs with exposed {110} facets are facilitated through hydrothermal route.[11, 33] The exposed facets are the highly reactive reaction places

for catalytic reaction.[34] These polyhedral IONCs could be synthesized by thermal decomposition method and hydrothermal method. In thermal decomposition process, adjusting the ratio of reactants, or just only changing the surfactant or solvent, IONCs with multiple polyhedral shapes and alterable sizes are obtained.[35] While, in hydrothermal method, metal cations and anions acted as the surfactants and stabilizers are the key parameters for controlling the polyhedral morphologies, such as cupric ion, zinc ion, 1-propanol and PVP, *etc*.[33, 36, 37] These ions or surfactants are served as similar functional tool as oleate in thermal decomposition method, providing controllable dynamics for nucleation and growth.

1D rods and wires. 1D IONCs including nanarods, nanorices, nanospindles and nanowires become the research focus, and these IONCs provide a good example to investigate the influence of dimensionality and size reduction on physical properties, especially the electrical transports and optical properties. 1D nanostructures of IONCs are formed by nucleation and subsequently anisotropic growth along a special direction (e.g. Z axis). While, in the growth process, choosing appropriate capping reagents (e.g. surfactant and additives) for kinetically control over the growth rates of various facets of a preformed seeds is a favorable way. For example, surfactants or additives are often used as adsorption agents to adsorb onto X and Y axis planes of IONCs because of the coordination or interaction of charges between preformed seeds and surfactants/additives, resulting in the selective growth of the preformed seeds along Z axis for anisotropic 1D IONCs.[38] Therefore, surfactant-assisted hydrothermal method becomes the effective route to produce 1D iron oxide nanorods, nanorices, nanospindles and nanowires. The regular surfactants and additives for synthesis of 1D IONCs during the surfactant-assisted hydrothermal process are presented in **Table 1**. Obviously, phosphate and amine are the preferential capping reagents for synthesis of 1D IONCs, which can be explained that the density of Fe atom on different facets is different and these anions are preferential bonding with the Fe atom. For example, density of Fe atom on the surface of {100} and {110} is higher than that on {001} facet, thus, the more preferential bonds of phosphate and amine onto {100} and {110} facets through covalent bonding are formed than that on {001} facet.[39, 40]

Table 1 Typical IONCs with 1D structure by surfactant-assisted hydrothermal method.

Nano-materials	Morphology	Iron source	Surfactant	Reference
α-Fe_2O_3	Nanospindle	$FeCl_3 \cdot 6H_2O$	$NaH_2PO_4 \cdot 2H_2O$	41-44
α-Fe_2O_3	Nanospindle, Nanorod, Nanotube	$FeCl_3 \cdot 6H_2O$	$NH_4H_2PO_4$	45, 46
α-Fe_2O_3	Nanospindle	$Fe(NO_3)_3 \cdot 9H_2O$	Ethylenediamine(EN)	47
Fe_3O_4	Nanorice	$FeCl_3 \cdot 6H_2O$	NaAc, Dodecyl trimethyl ammonium bromide (DTAB)	48
α-Fe_2O_3	Nanorod	$FeCl_3 \cdot 6H_2O$	Hexadecyl trimethyl ammonium Bromide(CTAB)	49
α-Fe_2O_3	Nanorod	$FeCl_3 \cdot 6H_2O$	Urea ($CO(NH_2)_2$)	50
α-Fe_2O_3	Nanorod	$Fe(NO_3)_3 \cdot 9H_2O$	Tetraethyl ammonium hydroxide (TEAOH) solution	51
Fe_3O_4	Nanorod	$Fe(CO)_5$	Hexadecylamine	52
α-Fe_2O_3	Hexagonal Nanorod	$FeCl_3 \cdot 6H_2O$	1,2-diaminopropane	53, 54
α-Fe_2O_3	Cantaloupe-like NCs	$FeSO_4 \cdot 7H_2O$	$NaClO_3$	55
α-Fe_2O_3	Nanowires	$FeCl_3 \cdot 6H_2O$	nitrilotriacetic acid (NTA)	56, 57

2D discs and prisms. The above mentioned 1D IONCs are formed by growing along [001] direction and blocking the growth directions of [100] and [110] by capping reagents. However, the 2D discs or prisms IONCs are formed by blocking effect of capping reagents on the [001] direction but growing along other two directions.[58] Generally, 2D discs or prisms IONCs are produced in hydrothermal process, while silicate anions and citric acid (CA) are the common capping agents for formation of discs and prisms IONCs because of their selective adsorption on {001} facet.[59] For example, layered single-crystalline α-Fe_2O_3 nanodiscs are synthesized by using silicate anions as a capping reagent to adsorb on {0001} facet of α-Fe_2O_3 seeds in hydrothermal route (**Figure 2a-c**),[60] triangular-like Fe_3O_4 nanoprisms are controlled by adjusting the ratio of solvent ethylene glycol (EG) and capping agent 1, 3-propanediamine (PDA) (**Figure 2d**),[61] hexagon Fe_2O_3 nanoprisms are fabricated by using citric acid (CA) as capping reagent, which can suppress the intrinsically anisotropic growth of hexagonal Fe_2O_3 NCs along the [0001] direction because of the chelating effect (**Figure 2e, f**).[62]

3D IONCs. Besides the aforementioned simple nanostructures, more and more 3D IONCs are prepared in recent years, such as nanoflower,[63, 64] nanostars,[65, 66] dendrite-like NCs,[67] nano-snowflake,[68, 69] peanut-like NCs,[70, 71] nanoworm,[72] urchin-like NCs[73] and airplane-like NCs.[74] These 3D IONCs possess hollow or mesoporous structures, providing larger specific surface area than 0D, 1D and 2D IONCs. Thus these 3D IONCs are beneficial to apply in sensor, catalysis and lithium battery.[63, 75] Most 3D structure of IONCs could be realized by hydrothermal process. And during this process, the precise size and shape of the formed 3D IONCs can be adjusted based on concentration of precursors, co-solvents, reagent ratios and surfactants or ligand choices.[76] For instance, the different ratio of solvents (isopropanol (IPA) and water) influencing the final morphologies of Fe_3O_4 NCs are shown in **Figure 3**. The star-shaped hexapods of Fe_3O_4 NCs are formed by using only IPA, and the concave-octahedrons of Fe_3O_4 NCs are formed in the addition of water into IPA solution. Meanwhile, the pH of reaction is also the main factor for controlling the morphologies of the 3D IONCs, six fold-symmetric snowflake-like and paired microplate-like α-Fe_2O_3 microstructure are synthesized in pH values of 12 and 14, respectively.[77]

2.1.2. Mesoporous IONCs

Mesoporous material is a kind of materials with pore diameter of 2-50 nm, as defined by International Union of Pure and Applied Chemistry (IUPAC).[78, 79] Comparing with the solid-structured IONCs, the IONCs mesoporous structured provide larger specific surface, symmetrical pore distribution and tunable size of pores. For example, the literatures report that the specific surface area of the commercial Fe_3O_4 NCs is 1.41 m^2/g, but this value for the mesoporous Fe_3O_4 NCs could reach to 47.7 m^2/g,[80] quasicubic α-Fe_2O_3 NPs with the size of 30-50 nm show the specific surface of 18.3 m^2/g,[81] but the porous Fe_2O_3 nanocubes with the size of 150-200 nm display much larger specific surface (44 m^2/g).[82] The typical mesoporous morphology of IONCs are shown in **Figure 4**. The mesoporous IONCs include 0D mesoporous nanospheres and nanocubes, 1D mesoporous nanospindles and nanorods, 2D mesoporous nanoplates and 3D mesoporous IONCs. These mesoporous IONCs could be obtained by template addition and removal,[83, 84] Ostwald ripening process[85, 86] or high-temperature calcination.[87-89] For

instance, a mesoporous Fe_3O_4 nano/microspheres are prepared by using hard templates method. During this process, poly(acrylic acid) (PAA) and SiO_2 are selected as the templates initially, and both of them are subsequently removed by calcining and etching process (**Figure 5a-e**).[90] Mesoporous Fe_3O_4 nanospindles are synthesized by sacrificed templates of α-Fe_2O_3 nanospindles. During this process, H_2 is employed as reduction agent to obtain Fe_3O_4 nanospindles from the α-Fe_2O_3 nanospindles, and the vacancies are remained in the Fe_3O_4 nanospindles after reduction **(Figure 5f-i)**.[91]

2.1.3. Hollow IONCs

Among various morphologies of IONCs, hollow IONCs are rapid-developed in recent decades, because the hollow IONCs with large specific surface areas exhibit a positive application prospect. The hollow IONCs not only present the unique properties, but also provide a broad range of applications such as photocatalysis, lithium battery, target drug delivery and sensors.[92-95] Hollow IONCs are classified into 0D hollow spherical/polyhedral structures, 1D hollow tubular/catenoid construction and 2D/3D complex hollow morphologies, and the typical morphologies of IONCs are illustrated in **Figure 6**. For synthesis of these hollow IONCs with special surface and interior structure, numerous of ways are proposed, such as hard/soft template,[96] *in suit* oxidation by using Kirkendall effect and Ostwald ripening process in hydrothermal method.[97-101] In this section, the general characteristics of hollow IONCs with various shapes and controlled process of their corresponding shape are investigated.

0D hollow spheres and polyhedrons. Generally, 0D hollow IONCs are formed through the aggregation of small grains, thus, the shell layer is accompanied with many pores. This characteristic of 0D hollow IONCs provides retainable space for series of materials (e.g. drugs) and passable route between interior and exterior through such pores of shell, providing promising applications of drug loading and releasing in biomedicine and coping the expansion space in lithium battery. These 0D hollow IONCs could obtain by template adding and removing process. The uniform removable templates are added in the reaction, then the reactants for synthesis of desirable IONPs shell layer are deposited or growth well onto these templates. Obviously, the morphology and dimensional uniformity of these hollow IONCs are highly dependent on the templates during this process. The thickness of IONCs shell layer could regulate by

the loading weight of precursors. The well-defined hollow iron oxide shell is obtained after etching or calcining the templates. For example, by employing carbonaceous polysaccharide spheres as templates, cage-like Fe_2O_3 nanospheres are synthesized *via* hydrothermal precipitation reaction. Then, the hollow Fe_2O_3 nanocages are obtained by removing carbonaceous polysaccharide spheres completely in annealing furnace at 500 °C for 4 h (**Figure 7a-e**).[102] Ostwald ripening in hydrothermal process is also another important way for formation of hollow IONCs. For example, hollow Fe_3O_4 NPs with size of ~400 nm are prepared by simple solvothermal method, the formation of hollow Fe_3O_4 NPs is under controlling by bubble-assisted Ostwald ripening, as illustrated in **Figure 7f, g**.[103]

1D hollow tubular/rods. Since the first discovery of carbon nanotubes (CNTs) in 1991, lots of efforts are devoted to synthesize inorganic nanotubes, particularly the tubular-structured IONCs by controllable ways.[104] 1D tube-like NCs demonstrate unique chemical and physical properties because of their large surfaces area of double-wall structure and low dimensionality. According to the present reports, tubular-structured IONCs could be classified into hollow nanotubes, nanowires, nanospindles and nano-dumbbells.[105-110] Normally, tubular-structured IONCs are formed basing on the hard/soft template, or scarified template strategies. In the hard/soft template strategy, lots of inorganic or organic nano-materials are employed as templates initially, and then these templates are removed to generate tube-like IONCs with nanoscale pore size. For example, 1D α-Fe_2O_3 nanotubes are produced by using CNTs as hard template.[111] Additionally, Ostwald-ripening process in hydrothermal method is a widely accepted route in synthesis of 1D hollow iron oxide nanotubes, such as the formation of α-Fe_2O_3 short nanotubes (SNTs).[15] During this Ostwald-ripening process, holes on the tip of the spindle are formed firstly, and then, the inner parts of the spindle gradually transfer to the outer surface through the hole, the hollow structure are formed finally.[109]

2D and 3D IONCs. Increasingly, IONCs with complex morphologies (such as 2D and 3D hollow IONCs) became eye-catching issues in recent years. For example, the 2D α-Fe_2O_3 nanorings are synthesized with high surface-to-volume ratio, exhibiting high sensitivity and good reversibility for gas-sensing of alcohol vapor under ambient conditions.[112] These 2D and 3D hollow IONCs possess larger

specific surface areas than hollow IONCs, therefore, various 2D and 3D hollow IONCs are synthesized successfully in recent years, including 2D nanorings[113-115] and hexagonal nanorings,[116] 3D nanobowls,[117-119] octahedral nano-framework[77] and multi-shelled nanostructure.[120] For synthesis of these 2D and 3D IONCs with different morphologies, ions-assisted Ostwald ripening in hydrothermal process is one of the most common way. For instance, hexagonal and dodecagonal α-Fe_2O_3 nanorings are prepared *via* double anion-assisted (F^- and SCN^-) hydrothermal method. The time-dependent formation process of hexagonal α-Fe_2O_3 nanorings is also under control of Ostwald ripening process, as evolved in in **Figure 8a, b**.[121]

2.2. Shape-dependent properties of IONCs

2.2.1. Magnetic properties of shape-controlled IONCs

Magnetic property of IONCs is an important characteristic for itself applications, but what are the factors and intrinsic reasons to influence the magnetic properties? From the standpoint of microcosmic, magnetic moment between each atoms and corresponding different interchange process are induced the different magnetic property of IONCs. The classification of these different interchange process is shown in **Figure 9a**.[122] Generally, diamagnetic IONCs is defined as the magnetic material without magnetic moment. When magnetic electrons keep far away from each other (no interchange process), then the orientation of atom magnetic moment of IONCs is randomly scattered and offset resulting in the paramagnetic characteristic of IONCs. The magnetic moments array is equal inverse parallel with existence of negative interchange process, resulting in antiferromagnetic characteristic of IONCs, while the magnetic moment is unequal inverse parallel, causing the ferrimagnetic nature of IONCs. Likewise, the parallel magnetic moments arraying with the presentation of positive interchange process produce ferromagnetic nature of IONCs. As a result, the magnetic property of IONCs could be classified into weak magnetic materials and strong magnetic materials, as illustrated in **Figure 9a**.

For testing the magnetic properties, a lot of common definitions of IONCs including saturation magnetization (M_s), coercivity (H_c) and remanence magnetization (M_r) are presented **Figure 9b**. These parameters of IONCs could be measured by Vibrating Sample Magnetometer (VSM) and

Superconductivity Quantum Interference Device (SQUID).[123] The simulative hysteresis loops (*M-H*) obtained by VSM are shown in **Figure 9b**. Form this simulative hysteresis loops, the definition of superparamagnetism, soft ferrites and hard magnetic ferrites could be revealed. The superparamagnetic behavior of IONCs present in curve a, (**Figure 9b)** while the *M-H* curve show no hysteresis at a certain temperature ($T > T_B$, blocking temperature). The forward and backward magnetization curves are overlapped completely.[12] The soft ferrites and hard magnetic ferrites can be defined according to the value of H_c and M_r. For example, the soft ferrites are stipulated when the H_c is less than 1×10^2 A/m and M_r is quite low (curve b in **Figure 9b**). While hard magnetic ferrites with higher H_c ($>1\times10^4$ A/m) and M_r than soft ferrites are presented in curve c of **Figure 9b**. Apparently, these typical parameters of magnetic properties such as M_s and H_c in various magnetite NCs are different. Because the magnetic property is influenced by the grain size, structural composition, shapes and surface anisotropy of the IONCs.[124] For example, α-Fe_2O_3 NCs generally show weak ferromagnetism and possess saturation magnetization less than 10 emu/g at 300 K.[36] But the saturation magnetizations of γ-Fe_2O_3 and Fe_3O_4 are extreme high (~ 92 emu/g) at same condition.[125]

Among all these factors, the size and shape of IONCs play important roles in magnetic property. The magnetic property of IONCs could be affected by different grain diameters.[126] Generally, the H_c of Fe_3O_4 NPs is extremely size-dependent parameter. For example, the H_c of IONCs increases rapidly with the grain size when the sizes of these IONCs are smaller than ferromagnetic exchange length (d_{ex}, $d_{ex}=\sqrt{A/K}$, A: denotes the exchange stiffness, K: an effective anisotropy constant). Because the H_c is in direct proportion to d^6 (d: the diameter of NPs). But if the grain size exceeds the d_{ex}, the magnetization reversal has happened because of domain wall motion. With the movement of domain walls through a sample, pinning occur between the boundary of two crystals, additional energy is needed for them to continue moving. The H_c is in direct proportion to d^{-1}. Hence, increasing the grain size will decrease H_c.[127, 128] The morphology-dependent magnetic property of IONCs are studied in recently.[129, 130] The H_c is easy to be affected by anisotropic shape, because more complex shape of

IONCs will inevitably increase the magnetic anisotropy, and the H_c of IONCs is considered to be the pinning effect in magnetic domain, which are induced by these magnetic anisotropies.[15, 131]

More recently, we have synthesized single and tubular clustered magnetite NPs (MNPs) by low-temperature coprecipitation and high-temperature hydrothermal in aqueous conditions, respectively. The sizes of the constitutive small NPs obtained from two methods are almost same. But the magnetic properties of two kinds of NCs are different. For example, the single MNPs show a superparamagnetic property at 300 K. However, the tubular clustered MNPs exhibit clearly ferromagnetic behaviors. Because the competition of the demagnetization energy of shape and the magneto crystalline anisotropy energy of small MNPs will increase the coercivity, then magnetic dipole-dipole interactions of assembled nanoparticle structures are much stronger than those of individual NPs. As a result, the distance-dependent nature of such interactions is proformed.[130] Moreover, α-Fe_2O_3 NCs with three different morphologies (single-crystalline NPs, dendrites and snowflakes) by hydrothermal reaction are also well demonstrated this point. The coercivities of single-crystalline (**Figure 10a**), dendrites (**Figure 10b**) and snowflakes (**Figure 10c**) α-Fe_2O_3 are gradually increased because of the growing number of OH^- ion on their surface. As a result, the surface spinning of α-Fe_2O_3 NCs are also increased. Subsequently, high coercivity of α-Fe_2O_3 NCs is produced since the spin relaxation mechanism is disturbed. Therefore, the anisotropic shape with surface-adsorbed OH^- ions is the main reason for variation of magnetic parameters. And the coercivity of α-Fe_2O_3 NCs increase with their anisotropic shape.[132]

2.2.2. Catalytic properties of shape-controlled IONCs

Catalytic property (including the catalytic oxidation and photocatalysis) is another important nature of IONCs, especially for the α-Fe_2O_3 NCs. α-Fe_2O_3 is a typical *n-type* semiconductor, which are widely used in heterogeneous catalysis and photocatalysis.[34, 133] In photocatalytic application, the electrons on the valence band (VB) of α-Fe_2O_3 NCs are excited to conduction band (CB) by absorption of photons, and the holes are left on the VB. These generated electrons and holes show the ability for photocatalytic

degradation of organic pollutant.[93] In catalytic oxidation, Fe sites on the surfaces α-Fe_2O_3 NCs should act as the active species for the catalytic oxidation reactions of CO and alcohols.[134, 135]

Generally,the catalytic property of α-Fe_2O_3 NCs is also shape-dependent. Different exposed facets and specific surface areas are the main factors for modulating the catalytic reaction efficiency.[136] For example, truncated-dodecahedron-shaped α-Fe_2O_3 NCs show a much higher photocatalytic degradation of Rhodamine B (RhB) than the rhombohedron-shaped α-Fe_2O_3 NCs. The high density surface exposed Fe ions (9.76 nm^{-2}) on the $\{10\bar{1}2\}$ facet endowed the truncated-dodecahedron-shaped crystals with superior photocatalytic activity in the photo-Fenton reaction than rhombohedron (surface exposed Fe ions density on $\{10\bar{1}0\}$ facet is 5.79 nm^{-2}).[137] Quasicubic and flower-like α-Fe_2O_3 NCs are synthesized for catalytic oxidation of CO. The quasicubic α-Fe_2O_3 NCs show a higher catalytic activities in CO oxidation than flower-like α-Fe_2O_3 NCs. The excellent catalytic property of quasicubic is attributed to the exposure of the {110} facets that have a much higher iron density (10.1 atoms nm^{-2}), which is facilitated to activate the CO.[81] This kinds of shape-dependent catalytic behavior of IONCs could be further investigated in liquid-phase catalytic reactions.[138, 139]

2.2.3. Gas sensing properties of shape-controlled IONCs

Gas sensing property is depicted as the responsivity of metal oxide semiconductors to various gases. The conductivity changes of metal oxide semiconductors could be detected in gas atmospheres. More specifically, gases could adsorb on the surface of these metal oxide semiconductors in the gas atmospheres, and capture electrons from the inner of the metal oxide semiconductors. A depletion layer is formed and thus the conductivity are correspondingly reduced.[140, 141] This mechanism could be found on the surface of some metal oxide semiconductors, such as ZnO, SnO_2, WO_3, *etc.*[142-145] Overall, the oxidation-reduction reaction occurs to these metal oxide semiconductors, and the conductivity changes.[146, 147] As the metal oxide semiconductor, IONCs also show the excellent gas sensing property for detection of various gases (e.g. methanol, ethanol and acetone, *etc.*).[63, 148-150] It is noteworthy that these IONCs show a general shape-dependent gas sensing property, which could be mediated by different exposed facets, specific surface areas and crystalline degree.[151, 152] For instance, α-Fe_2O_3 with

oblique parallelepiped and tetrakaidecahedral shapes show higher gas sensing property than other α-Fe_2O_3 with common shapes (less truncated degree polyhedral, more truncated degree polyhedral and quasi-spherical structure), because of the exposing higher energy facets of $(01\bar{1}4)$, $(10\bar{1}2)$ and $(\bar{2}110)$ in tetrakaidecahedral shapes. The higher density of the exposed Fe^{3+} cations of on those facets is beneficial to the reaction of gases and may provide active sites to adsorption of gas molecules.[153] Moreover, hollow α-Fe_2O_3 polyhedral exhibits higher gas sensing property than compact α-Fe_2O_3 polyhedral structures. Such a significant improvement of the sensing performance can be attributed to the contribution of the contact surface area between the hollow α-Fe_2O_3 polyhedral structures and the target gases.[154]

3. The synthesis of shape-controlled IONCs

3.1. Co-precipitation method

Co-precipitation method is a classical chemical route for synthesis of IONCs, especially for the Fe_3O_4 NCs. This method involves rapid titration of an acidic or neutral solution of Fe^{2+} and Fe^{3+} into an alkaline solution, resulting in rapid precipitation of particles. This chemical process is shown as follow:

$$Fe^{2+} + 2Fe^{3+} + 8OH^- \rightarrow Fe_3O_4 \downarrow + 4H_2O.$$

Precipitation of Fe_3O_4 NCs could be obtained under these conditions: the stoichiometric ratio of Fe^{3+}/Fe^{2+} is 2:1, and the pH of reaction should be alkalic condition (pH 8~14), then the reaction process is operated under atmosphere of inert gas. This method is a favorable method for producing IONCs in larger-scale. For example, Stroeve and co-workers synthesize Fe_3O_4 spherical NCs with mean crystal size of 8.5±1.3 nm in large-scale by using co-precipitation method under N_2 when fixed pH of 11 and without any surfactant.[155] However, the size distribution of IONCs products is broad in co-precipitation method because of no any surfactant present, which causes wide range of blocking temperature and limits their applications. Therefore, synthesis of Fe_3O_4 spherical NCs with narrow size distribution by co-precipitation method is still a challenge because of only kinetic factors are involved in this process.

Generally, the rapid nucleation and subsequent slow controlled growth are beneficial to obtain the monodisperse spherical NCs. As a result, controlling the nucleation and growth processes becomes the

key factor to produce monodisperse IONCs. In recent years, a modified co-precipitation method is proposed to synthesize monodisperse IONCs under controllable nucleation and growth process. In this process, organic additives are used as stabilizer and/or reducing agent for controllable nucleation and growth process. For example, ultrafine Fe_3O_4 spherical NCs with narrow size range of 4-10 nm are synthesized by co-precipitation method in the present of 1 wt.% polyvinlyalcohol (PVA) as stabilizer. Chain-like clusters precipitated Fe_3O_4 spherical NCs could be obtained when 0.1 mol % of hydroxyl groups in 1 wt.% of PVA are converted to carboxyl groups in the same reaction process.[156] Fe_3O_4 NPs with average size of 25 nm are synthesized by using octanoic acid as surfactant in a traditional chemical co-precipitation process.[157] These examples indicate that a proper surfactant could act as significant stabilizer or dispersant to synthesize monodispersed IONCs.

3.2. Thermal decomposition

To overcome the shortcoming of co-precipitation method, the thermal decomposition is proposed for synthesis of IONCs with accurately narrow size-distribution, monodispersed and multiple shapes. In thermal decomposition method, organometallic compounds are often used as precursors, such as iron acetylacetonates [$Fe(acac)_3$], iron cupferronates [$FeCup_3$], or carbonyls.[158, 159] And high-boiling organic agents including oleic acid (OA), 1-octadecene, 1-tetradecene and oleylamine are often added as solvents and stabilizers. Indeed, the ratios of the precursor, stabilizers and surfactants play the key role in size- and shape-controlling of IONCs. Especially the stabilizers, which not only play a role to slow down the nucleation process but also serve as an adsorption agent onto generated nuclei or growing NCs to hinder the growing facets. As a result, the IONCs with narrow size-distribution and isotropic/anisotropic morphologies are produced. For instance, spherical γ-Fe_2O_3 and Fe_3O_4 NCs with polysize (5 nm and 11 nm for γ-Fe_2O_3, 19 nm for Fe_3O_4) are prepared by thermal decomposition of $Fe(CO)_5$ in different molar ratio of $Fe(CO)_5$ and oleic acid (1:1, 1:2 and 1:3).[160] Because the high concentration of $Fe(CO)_5$ in reaction could propel more explosive nucleation of IONCs than the reaction with the low concentration of $Fe(CO)_5$ according to LaMer nucleation and growth theory.[161] In the growth process, lesser $Fe(CO)_5$ are left for growth of more primary nucleation. Thus, the size of the

IONCs increase with the decreasing of molar ratio of $Fe(CO)_5$ and oleic acid. Furthermore, the particle size of IONCs are easily controlled by using different kinds of solvent at different boiling points. For example, IONCs are synthesized by using inexpensive and nontoxic iron chloride as raw material to form the metal-oleate precursors. The IONCs with accurate sizes of 5, 9, 12, 16 and 22 nm are obtained by altering the boiling points of each solvent, such as 1-hexadecene (b.p. 274 °C), octyl ether (b.p. 287 °C), 1-octadecene (b.p. 317 °C), 1-eicosene (b.p. 330 °C) and trioctylamine (b.p. 365 °C).[162]

Additionally, thermal decomposition method is also a favorable way to prepare IONCs with different shapes, such as 0D nanocubes and nano-bipyramid. For instance, IONCs with different sizes and diverse morphologies are fabricated though thermal decomposition of iron oleate ($Fe(OL)_3$) precursors in the present of OA or oleate salts (**Figure 11a-c**). The spherical IONCs are synthesized by using the OA as surfactant, but the cubic IONCs are obtained by just replacing the OA with oleate salt (sodium oleate (NaOL) or potassium oleate (KOL)). Furthermore, the sizes of both spherical and cubic IONCs are increased with temperature rising (**Figure 11d-f**). Additionally, the bipyramidal IONCs are synthesized by only decreasing the molar ratio of oleate/$Fe(OL)_3$ (**Figure 11g**). Obviously, the surfactants of OA and oleate salts are facilitated the evolution of morphology of IONCs because of different adhesion ability of the OA and oleate on the different growing facets. Then, the cubic IONCs is a result of a slower growth rate of the {100} facets. Furthermore, {100}-bound bipyramidal NCs with a single (111) oriented twin plane are found by further adjustment of the growth conditions. This phenomenon are depended on several factors, such as heating rate and NaOL concentration.[163]

Althoughthe thermal decomposition of metal salt precursors is an effective way for monodisperse IONPs with a controllable size, the high boiling point organic solvents are required for obtaining the IONCs with hydrophobic surface, resulting in inevitable hydrophilic treatment process for further applications. In addition, these organic solvents also cause environmental contamination unavoidably.

3.3. Hydrothermal/solvothermal process

Hydrothermal/solvothermal synthesis is an accessible way for IONCs with various morphologies, which is involving the chemical reaction in an aqueous solution/organic solvent (in a sealed container)

under high temperature (130~250 °C) and high vapor pressure (0.3~4 MPa). During this hydrothermal process, the iron source and surfactants are dissolved in solvent or mixture to form ions or molecular groups for nucleation and growth at initial stage. The intense convection effects (producing by the temperature difference between the bottom and top of the sealed container) is the driving force for the transportation of these ions or molecular groups to growth sector (low temperature area) and generation of supersaturated solution until critical supersaturation for nucleation, resulting in large amount of magnetic nuclei. In the subsequent process, the dissolution and recrystallization process or Ostward repining are frequently induced in the growth of IONCs or the formation of hollow IONCs because of reducing the surface free energy. Moreover, such repeated dissolution and recrystallization are the critical processes for IONCs with high crystallinity. For example, α-Fe_2O_3 NCs with polyhedral shape are prepared by using $FeCl_3 \cdot 6H_2O$ and ammonia water as precusors and water as solvent in hydrothermal process under 180 °C for 8 h.[164] Moreover, Fe_3O_4 NCs could also be synthesized by using these precusors and solvent, but with the addition of sucrose as reductant for reducing the Fe^{3+} into Fe^{2+}.[165] For preparation of γ-Fe_2O_3, oxidation of the Fe_3O_4 NCs to form γ-Fe_2O_3 counterpart is a common way.[166, 167]

In the hydrothermal process, water or solvents are important parameter in wet-chemical reaction, different solution can produce IONPs with different shapes. Water is not only serve as solvent but also play a chemical component to take part in a chemical reaction. Additionally, the other organic solvents including EG, diethylene glycol (DEG), glycerol are the fashionable solvents in the solvothermal process. Other parameters, such as temperature, pressure, pH value and ion adding, are also the common alterable parameters for controlled morphologies, sizes and crystal structures of these IONCs. For example, in our previous work, we prepare α-Fe_2O_3 NCs with various morphologies (short nanotubes, NPs and nanorings) by using anion-assisted hydrothermal method. Then the shape evolution of α-Fe_2O_3 NCs with the Fe^{3+} concentration and time-dependent process is presented in **Figure 12**. Obviously, the performed hollow structure of these α-Fe_2O_3 NCs become more evidently when the reaction time is prolonged. Furthermore, the morphology of the α-Fe_2O_3 NCs is evolved from hollow sphere to hollow

nanotube with the increase of Fe^{3+}. The shape of the short nanotubes is mainly regulated by the adsorption of phosphate ions on parallel facets to the long dimension of elongated α-Fe_2O_3 NPs (axis) and the hollow structure is performed by the preferential dissolution along the c-axis because of the strong coordination of the ions.[168, 169] Obviously, the IONCs prepared by hydrothermal/solvothermal method show some superior advantages, such as high purity, high dispersion, shape-controllable and environmentally friendly.

3.4 Microemulsion

Microemulsion is a transparent/translucent isotropic dispersion and thermodynamical stability solution, which is formed by two immiscible liquids, such as water and oil. These two kind of bulk solutions are formed individual micro-droplets (typically 1-50 nm in diameter). These individual micro-droplets are also named as micelle, which are stabilized by interfacial film of surfactant molecules in microemulsion. In preparation of nanomaterials by this microemulsion method, the different individual micelles are typical nanoreactors for material-exchanges of two or more kinds of reactants, the nucleation and growth process are both happened in the nanoreactors. The final NCs are extracted by filtering or centrifuging when the demulsifying agent (acetone or ethanol) are added in. Microemulsion as a nanoreactor could be used in synthesis of various nanomaterials with uniform sizes and multiple composites, such as metallic cobalt, cobalt/platinum alloys, and gold-coated cobalt/platinum NPs.[170]

Additionally, for synthesis of IONCs, microemulsion method is also a good choice. The different reactants (such as iron source, alkali solution) in same water-in-oil microemulsions are mixed for precipitation of IONCs through continual micelle collision coalescence and re-break process.[171] Generally, the size of final IONCs are depend largely on the size of the micelle. In the micelles collision, coalescence and re-break process, the size of micelle is mainly dependent on the property and dispersity of microemulsions, such as the ratio of water/oil, the amount of surfactant and stirring rate. For example, IONCs with average diameters of 3, 6 and 9 nm are prepared by microemulsion method at room temperature. The IONCs were stabilized *in situ* by organic surfactant molecules (polyoxyethylene (5) nonylphenylether), which acted both as a stabilizer for the microemulsion system and as a capping layer

on the surface of the IONCs. The size of these IONCs could be regulated by the volume ratio (organic + water/surfactant) and stirring rate.[172] This method provides a lot of advantages in preparation of IONCs as comparing with other methods. For example, the synthesized spherical IONCs present uniformed size distribution and hydrophilic surface for *in vivo* biomedicine or biodiagnose.[173]

Though many IONCs with different sizes are synthesized by using microemulsion method, how to control the morphology of IONCs is still a distinct shortcoming. At present, only spherical or quasi-spherical IONCs are the available products through this microemulsion method because of the micelles is spherical. Additionally, how to increase the yield of IONCs is another challenge by employing this method. Moreover, in order to synthesize appreciable amounts of material, a lot of organic solvents are required in the microemulsion, which is against with the protocol of environmental protection.

4. Proposed mechanisms for shape-controlled IONCs

4.1 Ostwald ripening

Originally, Ostwald ripening is a phenomenon happened in solid-solution state that particles with inhomogeneous size change over time. In other words, the large particles grow up by sacrificing the dissolved small particles because of their different size-dependent solubility. For example, the chemical equilibrium of particles with different size is established between the solid-solution interfaces in a certain reaction condition.[174] Ostwald ripening is a coarsening process of NPs, the preliminary particles with different size are suspended through homogenous solute, the concentration of the molecules around the interface of smaller particle is larger than the average concentration in bulk solution because of the capillary effect. This concentration gradient drive the small particles dissolving and vanishing, causing the increase of local molecules concentration. These molecules with high concentration are diffused to surr ounding of bigger particles. As a result, homogenous concentration will eventually proceed for the growth of bigger particles and elimination of smaller particles.[175] This phenomenon was first described by Wilhelm Ostwald in 1896.[176] Previously, Ostwald ripening is generally found in water-in-oil emulsions.[177] But in recent year, this phenomenon could also be found in polar solvents during hydrothermal process for synthesis of nanomaterials.[178]

In hydrothermal route, two basic steps are involved for IONCs: nucleation and particle growth.[58] During the particle growth process, Ostwald ripening play an important role in forming large particles or mesoporous/hollow structures of IONCs by aggregating the smaller crystallite particles.[179, 180] For synthesis of solid IONCs, large IONCs are growing at the expense of small IONCs, resulting in an increase of particle size but a decrease of the number of particles. In the formation of mesoporous/hollow IONCs, the inner smaller crystallites are produced at the early stages of nucleation and growth, and then these small primary crystallites random aggregate in the inner place before the growth of external crystallites. Under high temperature and high pressure conditions, the central region of the spheres start to be evacuated *via* dissolution because of their higher surface energy.[181] Then, the inner dissolved smaller crystallites are transformed from interior to exterior of the spherical IONCs and formed a stable mesoporous/hollow structure with better crystallinity.[182] These two processes are both driven by reduction of the surface free energy. The small particles with high surface free energy are unstable, resulting in high inclination for more stable structure. For example, aggregated α-Fe_2O_3 nanoplates are formed with adding of ionic liquid [Pmim]I in a hydrothermal route. Three steps are proposed for the formation mechanism: nucleation, growth/self-assembly and Ostwald ripening. During Ostwald ripening process, the aggregated α-Fe_2O_3 nanoplates are coalesced by small nanoplatelets.[183] Hollow cocoon-like α-Fe_2O_3 nanospheres are synthesized by one-pot hydrothermal method without any surfactants. With prolongation of reaction time, the hollow cocoon-like α-Fe_2O_3 nanospheres are formed under the Ostwald ripening process (**Figure 13a, b**).[184] Moreover, the evolution of morphology of IONCs is a time-dependent process. With prolonging the reaction time, small and unconsolidated primary crystallites could dissolve out and the IONCs are available to reconstitute into different morphologies and more stable structures.[185]

4.2 Oriented attachment

Oriented attachment was first proposed by Penn and Banfield in synthesis of TiO_2 NPs since 1998, referring that the existed primary crystallites are attached in a specific direction gradually for oriented reconstruction in solution to assemble into single crystalline NPs.[186, 187] In other words, primary

crystalline grains are served as building blocks for aggregating into larger size or more complex morphology, the adjacent primary crystalline grains are self-assembled into bigger particles by sharing a common crystallographic orientation, and subsequent docking of their crystal facets.[188] From the thermodynamic viewpoint, the driving force for this spontaneous oriented attachment is that the disappearance of two high energy surfaces lead to a substantial reduction of the surface free energy.[189] Recently, the directly observation of Oriented attachment process of iron oxyhydroxide NCs is performed on high-resolution transmission electron microscope (HRTEM) by using a fluid cell, revealing that a perfect lattice match between attached NCs is a vital step for crystal growth by Oriented attachment.[190]

By employing this Oriented attachment mechanism, a lot of anisotropic-shaped nanostructures could be synthesized *via* fusion of their primary NCs,[191, 192] such as α-Fe_2O_3,[193, 194] Fe_3O_4,[195] SnO_2,[196] and TiO_2,[197] *etc.* Actually, the structures and shapes of primary "building blocks" act a significant role in Oriented attachment growth and the formation of products. Because the primary units may completely or partially keep the original structure and configurate during the process of Oriented attachment growth.[198] Moreover, the difference of surface energy at each facet leads to the coalescence of primary particles in specific crystallographic orientation, such as the one-dimension growth in [001] direction of TiO_2 nanorods and in [100] direction of PbSe nanowires by using the primary unit with the same polyhedral shape.[190, 200] Generally, Oriented attachment of IONCs is facilitated for various morphologies,[201, 202] such as cubes,[81] oblique,[203] nano-cantaloupe[55] and hierarchical nanostructure,[204] *etc*. These morphologies are influenced by each primary unit. For example, Goethite (α-FeOOH) nanorods are formed by oriented aggregation of the goethite primary NPs.[202] Well-defined cubic hematite (α-Fe_2O_3) single crystals grow up from the primary crystallites of free-standing α-Fe_2O_3 nanorods. This formation process of these cubicα-Fe_2O_3 single crystals is explained in terms of oriented attachment. Firstly, nanorods are aggregated in orientation on the surfaces of some cores by sharing the common facet of {012}. Then, the polycrystalline NCs would fuse into a single crystal *via* Oriented

attachment mechanism. Eventually, the well-defined cubic hematite single crystals are formed, as shown in **Figure 14a, b**.[205]

4.3 Selective adhesion induced anisotropic growth

Surface energy is a vital factor to affect the anisotropic growth of IONCs. Generally, the crystal growth rate is in proportion to the surface free energy of each facet.[206] In a certain crystal facet, the faster growth rate would induce the easier disappearance of this facet. Thus the final shape of IONCs is highly dependent on the facets with slowest growth rate. For instance, the calculated surface energies of hematite based on density function for {001}, {101}, and {104} facets are 1.146, 1.308, 1.453 J/m^2, respectively.[207] If a polyhedral α-Fe_2O_3 primary crystallites possess with only these three exposed facets, then {104} facets are easier to disappear in growth process because of their faster growth rate. Thus the {001} facets are eventually exposed in final product. But in fact, most of final IONCs are sphere with the lowest surface free energy, because only kinetics control is presented in the growth process after nucleation.

In recent decades, surfactants or additives are found as capping-agents for controlling the shapes of IONCs. Many literatures reveal that a selective adsorption of surfactant or additives on a certain facet is a sensible and effective way for regulating the growth rate. Functional groups of surfactants or additives molecules as attachment point can selectively absorb on specific facets of primary IONCs crystallites by coordination or interaction of charges because of the different properties of each facet (coordinative bond, charged facets or electrically neutral but dipolar), then the surface energy are reduced subsequently. As a result, the selective facets are blocked for growing inhibition, and these facets are finally exposed in obtained products.[208, 209] Lots of surfactants or additives are considered as crystal growth inhibitor adhering on special facets for synthesis of IONCs, such as phosphate,[210] hydrogen phosphate,[211] fluorid,[212] EDTA[213] and oleylamine[214] *etc.* These surfactants or additives are able to coordinate with Fe^{3+} on a certain facets of preformed IONCs nuclei because of the crystal anisotropy and the limited amount of these anions,[45, 112] thus the concentration of these surfactants or additives is also the influence factor for further controlling the shapes of IONCs.[212, 215] For example, IONCs with

1D and 2D shapes are synthesized by using different surfactants or additives as capping reagent for adsorption of on different facets. For synthesis of 1D IONCs, phosphates are used to adhere onto (100) and (110) facets of primary crystallites selectively, thus the growth direction of these 1D IONCs is [001] direction, the α-Fe_2O_3 nanospindles are finally formed (**Figure 15a**).[58, 216] However, surfactant oleylamine is tend to bind onto the surfaces of $(00\underline{1})$, causing the growth directions along [100] and [110] for Fe_3O_4 nanoplates (**Figure 15b**).[214]

3.3 Nanoscale Kirkendall effect

Conventionally, Kirkendall effect is a motion of boundary layer between two metals, which is induced by the different indiffusion rates of the metal atoms. This phenomenon was first proposed from copper and brass (zinc) system by Smigelkas and Kirkendall in 1947.[217] More recently, Kirkendall effect is developed for synthesis of hollow nanomaterials. Different from this conventional Kirkendall effect, nanoscale Kirkendall effect is found in interface of a core-shell nanostructure, as presented by Co_3S_4 hollow NPs.[218] The indiffusion rate of the core material is higher than shell one, causing migration from the core to the shell for hollow structure of materials in nanoscale. As such, diverse of nanomaterials with hollow structures including CoM (M=O, S, Se),[219-221] Al_2O_3,[222] CdS, [223] Ni_2P,[224] and NiO,[225] *etc.* are produced with the controlled nanoscale Kirkendal effect.

Furthermore, the nanoscale Kirkendal effect is also an effective and fashionable mechanism to prepare hollow IONCs. Generally, the hollow IONCs are formed through an oxidization process of iron salt precursor. The core iron NPs are exposed to oxygen for growth of iron oxide shell, and the hollow iron oxide shells are formed, because the diffusion rate of iron is faster than the oxygen. For example, the outward diffusion rate of Fe metal is faster than the inward diffusion rate of oxygen, then the IONCs are collected at the interface of metal-oxygen. During this process, the unbalanced interfacial diffusion between oxygen and Fe atoms is the key role for hollow IONCs.[226] In addition, by altering the experimental parameters, such as reaction time and temperature, the oxidation process is available to obtain core-shell, rattle-type and hollow nanostructures. For example, Alivisatos and co-workers fabricate the hollow Fe_3O_4 NCs by exposing the iron NPs to dry 20% oxygen for different time and

temperature. Different diffusing rates of Fe and O elements caused the formation of voids between the Fe core and the Fe_3O_4 shell. With the prolonging of exposed time and raising the temperature, the outside-in oriented oxidation happens on the preformed core-shell Fe@Fe_3O_4 NPs for different morphology of IONCs (**Figure 16a-e**).[97] During these diffusion, Fe NPs are vanished instead of the appearance of Fe_3O_4 shell, which are the typical products by nanoscale Kirkendall effect. Not only the hollow spherical of IONCs can be synthesized by this method, but IONCs with other morphologies including hierarchical porous iron oxide films, nanotubes and porous hollow NPs are also prepared.[99, 227, 228]

3.4 Self-assembly

Self-assembly is a process that small NPs or other discrete components spontaneously are organized because of direct specific interactions. The NPs, nanowires, nanorods and nanotubes are served as structural unit to assemble into large nanostructures in 1D, 2D and 3D space.[229, 230] As a result, such aggregative crystals with thermodynamical equilibrium and minimum system free energy are finally obtained. Furthermore, the non-covalent interaction between structural units is the main driving force for stable morphologies of the self-assembled crystals.[230] It is noteworthy that the occurrence of self-assembly is a spontaneous process without other driving forces (such as high pressure or high temperature).[231] Then, such spontaneous self-assembly process is facilitated for IONCs with various anisotropic morphologies including NPs,[232] nanoclusters,[233] nanocubes,[234] nanorings,[235] mesoporous nanofilms[236] and hollow NPs.[237]

More recently, 3D urchin-like and flower-like IONCs are prepared in hydrothermal process *via* self-assembly mechanism, different iron sources and solvents play key roles in morphology controlling. For example, self-assembled urchin-like iron hydroxide and iron oxide NCs are synthesized in large-scale by using $FeSO_4$ as iron source and water/ethanol as solvent. SO_4^{2-} has stronger coordination with the iron ion than other ions under sonication in the formation of 3D self-assembled nanostructure.[238] Furthermore, novel 3D flowerlike iron oxide nanostructures are prepared *via* self-assembled process in

EG solvent. The iron oxide precursor could be obtained in refluxed EG solution by employing the $FeCl_3$ as iron source. The growth in three steps with self-assembly are shown in **Figure 17**.[239]

5. Energy conversion application of IONCs with various architectures

Electrochemical performances of IONCs with various architectures and high tailorabilities have attracted a lot attention in recently. IONCs with these performances provide more opportunity for energy conversion application. The energy conversion refers to the electric energy, which is transferring from one object to another, or from one form to another. Photoelectric effect and charge transfer principles are the main theories of these IONCs to apply in energy conversion application. These energy conversion applications, such as the photoelectrochemical water splitting, DSSCs and LIBs electrode, have attracted lots attentions.[171, 240] The special morphologies make to these IONCs become excellent materials for conversing optical/chemical energy to chemical/electric energy. Furthermore, different morphologies of IONCs show significant effect in different applications. Hence, in this section, the shape-dependent energy conversion applications of IONCs are investigated briefly.

5.1 Photoelectrochemical water splitting

Photoelectrochemical water splitting is proposed to be a promising method for hydrogen energy storage. In terms of mechanism, the photoelectrochemical water splitting process is a typical energy conversion process, which is involving the transformation of solar energy to chemical energy. Detailedly, photoelectrochemical water splitting consist of three processes: (1) the photo-excitation of electron-hole pairs, (2) the transfer of carriers to the electrode surface, and (3) H_2 and O_2 production by reducing and oxiding water on the different electrode surface.[241] Metal oxide semiconductors including IONCs, are the typical photocatalysts for photoelectrochemical water splitting. α-Fe_2O_3 is a typical *n-type* semiconductor with a band gap of ~2.2 eV, which possess a wide optical absorption cover substantially all the visible spectrum. Thus, these α-Fe_2O_3 could absorb photons of visible light, and convey them to electric energy (electrons and holes), these electrons and holes show the ability for splitting water into H_2 and O_2.

In general, the substrate is used for deposition or growth of α-Fe_2O_3 films or arrays, and a transparent conductor such as fluorine doped tin oxide (FTO) is acted as substrate. The different morphology of these deposited or growth α-Fe_2O_3 layers could result in different photoelectrochemical performance. In practice, the thin iron oxide films are found to exhibit poor performance because of the increased recombination of the photogenerated electrons and holes.[242] More recently, the α-Fe_2O_3 layers on substrates with novel morphologies are synthesized for enhancement of photoelectrochemical performances, such as porous thin films, nanowire arrays, nanotube arrays, and tree fork-like arrays.[243-246] These α-Fe_2O_3 layers are endowed with both larger surface area and crystal plane orientation induced fast electron transport path. For example, ultrathin (5-7 nm thick) Fe_2O_3 nanotube arrays (3-4 μm long) on Fe foil are synthesized for splitting water to generate hydrogen under solar light illumination. The obtained photoactivity of Fe_2O_3 NTs (1.4 mA/cm^2) is found to be higher than the nanoporous Fe_2O_3 (0.26 mA/cm^2), and Fe_2O_3 NPs (0.004 mA/cm^2). The better photoactivity of Fe_2O_3 NTs arrays could be attributed to a faster charge transfer through the nanotubes compared to the NPs.[27] Therefore, during the synthesis process, α-Fe_2O_3 layer with larger surface area and pore structure is favorable for improving the photoelectrochemical performance, and these structure could be realized by controlling the synthesis conditions.

α-Fe_2O_3 NCs with various morphologies as a kind of promising photocatalysts show their unique merit in hydrogen storage application. Such as low-cost, high photocorrosion resistant, high utilization rate of visible light and stable chemical properties,[247, 248] *etc.*, which bring feasible application in hydrogen storage. However, the highly photoelectrochemical performance in theory of α-Fe_2O_3 NCs cannot be reached, because it is restricted by many factors, such as poor electron conductivity, short mean free-path of holes (2-4 nm), slow kinetic process of O_2 production on surface of α-Fe_2O_3 NCs and high recombination rate of electron-hole pairs.[249-251] Thus, improving strategies for the photoelectrochemical performance of α-Fe_2O_3 NCs becomes the urgent affair in hydrogen storage application. Although main efforts are made in morphological control, ion doping and surface modification for improving the photoelectrochemical performance,[247, 252, 253] the photoelectric efficiency

is still maintained at a low level. In the future, improving the photoelectrochemical performance is still a research focus, and it is necessary to study the photoelectrochemical mechanism of IONCs for further improving the photoelectrochemical performance.

5.2 Dye-sensitized solar cells

In recent years, DSSCs are the representation of the third generation of solar cells, and it gain widespread attention. Because this kind of cells provide compatibility with low production costs, ease of fabrication and high photon-to-electron conversion efficiency.[254] It is an excellent candidate for new generation of clean energy storage. In general, a standard DSSCs consists of a dye-sensitized work photoanode, an electrolyte containing the redox couple (such as I^-/I^{3-}) and a counter electrode (CE).[255] Anatase-type TiO_2 films or arrays are first employed as a photoanode for DSSCs because of its photochemical stability and high photovoltaic performances. Nevertheless, large band-gap (3.2 eV) of TiO_2 is the shortcoming for full spectrum absorption, because the electrons are photoexcited only by UV light (<400 nm in wavelength), which occupies only 5 % of the solar light.[256, 257] More recently, α-Fe_2O_3 films or arrays are also shown a good photovoltaic performances for application in DSSCs. As a narrow band-gap semiconductor, α-Fe_2O_3 exhibits broader photo-response in the visible region.[258] During the photoelectrochemical reaction, larger surface area of the α-Fe_2O_3 films or arrays positive electrode provide more sites for absorption of dye molecules, such as flower-shaped α-Fe_2O_3.[259, 260] Thus the photon-to-electron conversion efficiency is influenced by the morphologies of synthesized α-Fe_2O_3 in some degree. For instance, the α-Fe_2O_3 nanorods array and NPs are used as anodes for DSSCs application. The DSSCs performance based on the optimized α-Fe_2O_3 nanorods array reaches a conversion efficiency of 0.43%, which is higher than α-Fe_2O_3 NPs (0.29%) under the light radiation of 1000 W/m^2.[261]

More interestingly, α-Fe_2O_3 are explored as CE for DSSCs application in recent years, because the literatures reveal that the performance of DSSCs is found to be related to their CE behavior.[262, 263] The function of a CE in the DSSCs is collection of electrons from the external circuit, and providing a path for electron transfer from the CE interface to the electrolyte by reduction of tri-iodide ions (I^{3-}). The

reactive activity of CE is usually affected by various factors such as specific surface area, porosity and crystal plane orientation.[264] The morphology of CE materials can act as an effective factor in improving the catalytic activity in a DSSCs. Similarly, the morphology of the α-Fe_2O_3 is also the significant factor for influence the photovoltaic performances in DSSCs.[265] For example, α-Fe_2O_3 NCs with different morphologies such as NPs, nanofibers, nanoflowers and nanorods was successfully fabricated *via* hydrothermal reactions and introduced into DSSCs as CE. α-Fe_2O_3 NPs CE exhibit the best reactive activity of reduction of I^{3-} among all these α-Fe_2O_3 NCs, and a maximum conversion efficiency of 4.60% is obtained. This superior efficiency may be attributed to the larger surface area of NPs and their crystal structure which has grown in [012] and [104] directions.[266]

Although the α-Fe_2O_3 NCs with larger surface areas are widely used as dye-sensitized work photoanode and CE in DSSCs application. The energy conversion efficiency of pure α-Fe_2O_3 NCs is still very low (0.1%) because of the fast electron-hole recombination, small optical absorption coefficient and low carrier mobility.[267, 268] The ultrafast recombination of the photo-generated carriers (time constants ~10 ps) along with the poor minority charge carrier mobility (0.2 cm^2 V^{-1} s^{-1}) leads to a short length (2-4 nm) of hole diffusion.[269] Therefore, coupling of α-Fe_2O_3 NCs with other semiconductors is a effective way to improve the energy conversion efficiency. Because fast charge transfer in the interface between these semiconductors is obversed.[270, 271] We believe that fabrication of these composite nanostructures in DSSCs application is the tendency in the future.

5.3 Lithium ion batteries (LIBs)

Nowadays, iron oxide materials are the great potential choice for realization of high performance LIBs. The chemical energy could be converted into electric energy when these iron oxide materials acted as the electrode in LIBs application. However, bulk Fe_2O_3 electrodes exhibit the poor cycle performance because of their low electrical conductivity, serious hysteresis between charge and discharge potentials. Poor capacity retention during cycling is caused by large volume change and unstable solid electrolyte interphase formation, especially at high current densities. Thus, nano-sized iron oxide materials are employed as anode materials in application of LIBs, because these nano-sized

materials can assuredly shorten the Li^+ transmission path, and promote the activity of the electrode contact area because of their unique properties.[272, 273] With the further investigation for anode materials of LIBs, IONCs are the good candidates for anode materials of LIBs. For example, transition metal oxide α-Fe_2O_3 has attracted much attention because of its large specific capacity (1007 mAh/g), which is higher than the common commercial graphite (370 mAh/g), and also provide characteristic of low-cost and environmental friendly.[274] During the charge-discharge process, the IONCs are reduced into Fe and Li_2O, then, an oxidation process of Fe to Fe_xO_y, are also happened during the electrochemical cycling, these cyclic process are shown as followed:[275-277]

$$Fe_2O_3 + 6Li^+ + 6e^- \leftrightarrow 2Fe + 3Li_2O$$

$$Fe_3O_4 + 8Li^+ + 8e^- \leftrightarrow 3Fe + 4Li_2O$$

Though IONCs are the most promising materials for electrode in LIBs practical application. The electrochemical performances of these IONCs based electrode prepared based on these IONCs are still influenced by many factors, such as specific surface area. Larger specific surface area is a favorable factor for improving the electrochemical performances of IONCs. By compared with the inferior performances of solid IONCs, mesoporous and hollow IONCs are commonly used as anode materials for high-rate lithium batteries application, because of the larger specific surface area. For example, the spindle-like mesoporous α-Fe_2O_3 with large specific surface area (75 $m^2\ g^{-1}$) exhibit the excellent Li storage properties with a higher reversible capacity by compared with another spindle-like α-Fe_2O_3 (synthesized by different condition, specific surface area is 37 $m^2\ g^{-1}$). This high-performance could be ascribed to the nanometer-sized subunits with larger specific surface area, which possess more activity sites and shorten distance for transportation of Li ions. More interesting, the hollow or pore structure allows the electrode materials to buffer the volume change during the discharge-charge process, and it is another favorable factor for this enhanced performance. Xie and co-workers fabricate hollowh ematite spheres for lithium-ion battery application. The improved discharge capacity is obtained (1279 mAh/g) at a current density of 60 mA/g.[278] Therefore, in synthesized process, precise controlling the synthesis

condition for obtaining the IONCs with hollow or pore structure are the essential requirement for achieving the stable electrochemical performances.

However, there are still some problems have to be faced by using pure IONCs as anode materials, such as low electric conductivity, pulverization caused by large stress and volume changes during charge/discharge processes, and aggregation of IONCs during the cycle process (because of their large surface area and activity). These problems hinder the practical application of pure IONCs in LIBs. With the development of energy storage research of iron oxide nanomaterials, we believe that these problems could be solved.

6 Summary and perspectives

Shape-controlled IONCs with various morphologies are developed for many years. The magnetic properties and energy conversion applications are mostly the shape-dependent characteristic. This review summarizes some classified characteristics of shape-controlled IONCs and their shape-dependent magnetic properties. The synthesis routes, formation mechanisms and energy conversion applications of these IONCs are also described. Generally, the characteristics of these IONCs with various morphologies (large specific surface, high surface energy and high activity reaction sites) are realized based on the controllable synthesis process and shape-controlled mechanisms, then the shape-dependent magnetic property of IONCs is illustrated subsequently. Based on existing plentiful literatures, this review provides a basic and integrated shape-controlled processes and consequences of IONCs to understand the relationship between morphologies and their corresponding magnetic property and applications.

Recently, the IONCs with various shapes (solid, mesoporous and hollow) for diversified applications are developed. Indeed, IONCs with more complex structures such as bionic structure is became one of the hottest applications in recently. However, there still are some unconquered problems of these IONCs in various applications, such as low light utilization and light-conversion efficiency in photoelectrochemical water splitting and DSSCs application, low electric capacity and high preparative costs in LIBs application. These unresolved problems will provide new research directions in the future.

Furthermore, with the furtherance of research in fabrication technologies of nanomaterials, the in-depths application of IONCs with diversified features will develop to a variety of areas in the future. More favorable morphologies of IONCs with superior properties would be discovered with the progression of the new mechanisms during controllable and tunable synthesis process; Many properties such as photoelectrochemical, electricity-storage properties are developed to raise for practical industrial applications. In summary, extensive applications of the multifunctional IONCs will be the most attractive issues in various field for a long time.

Acknowledgments

This work was partially supported by the NSFC (51201115, 51471121, 51171132, 11375134), China Postdoctoral Science Foundation (2014M550406), Hubei Provincial Natural Science Foundation (2014CFB261), Natural Science Foundation of Jiangsu Province (BK20160383), the Fundamental Research Funds for the Central Universities and Wuhan University.

Author Biography

J. Liu

Jun Liu received his B.S. in 2011 from Hengyang Normal University (Hunan, China). He received M.S. in 2014 from Hunan University of Technology (Hunan, China). Now he is a PhD candidate with a major of material physics and chemistry in Department of Physics at Wuhan University (Hubei, China). His research is focused on the design and synthesis of various iron oxide nanomaterials for diversiform energy conversion applications.

Z. H. Wu

Zhaohui Wu received her B. Sc (2007) and M. Sc on Biomedical Engineering (2011) from Hunan University of Technology (Hunan, China). Her major topic was morphology and structure control of magnetic nanoparticles and biology application of functional magnetic nanoparticles during the M. Sc. She is a PhD student in Chemical Engineering, Kyung Hee University, Korea. She is currently researching on the crystallization process controlling and product quality design including morphology, size and purity of organic crystals or inorganic nanoparticles. Her multidisciplinary research involves inorganic/organic materials design through crystallization process and application of nanomaterials in biomedicine and functional devices.

W. Wu

Wei Wu received his PhD in 2011 from the Department of Physics, Wuhan University, China. He then joined the group of Prof. Daiwen Pang at Wuhan University (2011) and Prof. V. A. L. Roy at City University of Hong Kong (2014) as a postdoctoral fellow. Now he is the Director of Laboratory of Printable Functional Nanomaterials and Printed Electronics, School of Printing and Packaging, Wuhan University. He has published over 70 papers, which have received over 1200 citation. He is also the editorial board member of *Advanced Science, Engineering and Medicine* and *Journal of Green Science and Technology*, his research interests include the synthesis and application of functional nanomaterials, printed electronics and sensors.

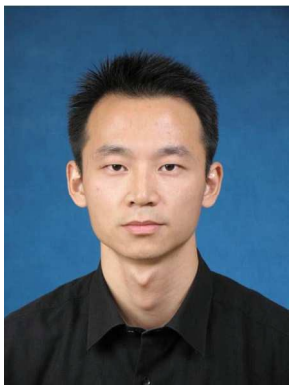

X. H. Xiao

Xiangheng Xiao obtained his B.S. in 2001 and PhD in 2008 from Wuhan University. Currently, he has been a full professor in the Department of Physics, Wuhan University since 2015. The research fields are mainly focusing on surface-enhanced spectroscopy, nanophotonics and ion beam modification of nanoscale material devices. Over 90 publications have been released in journals including *Advanced Materials*, *Nano Letters*, *Light: Science & Applications*, *Advanced Functional Materials*, *Nano Research*, *Nanoscale*, *Scientific Reports*, *Applied Physics Letters*, *etc*.

References

1. H. Gleiter and P. Marquardt, *Z. Metallkd.*, 1984, **75**, 263-267.
2. F. Hu, L. Wei, Z. Zhou, Y. Ran, Z. Li and M. Gao, *Adv. Mater.*, 2006, **18**, 2553-2556.
3. P. L. Taberna, S. Mitra, P. Poizot, P. Simon and J. M. Tarascon, *Nat. Mater.*, 2006, **5**, 567-573.
4. W. Wang, J. Y. Howe and B. Gu, *The J. Phys. Chem. C*, 2008, **112**, 9203-9208.
5. D. K. Zhong, J. Sun, H. Inumaru and D. R. Gamelin, *J. Am. Chem. Soc.*, 2009, **131**, 6086-6087.
6. M. M. Rahman, A. Jamal, S. B. Khan and M. Faisal, *J. Nanopart. Res.*, 2011, **13**, 3789-3799.
7. M. Morales, S. Veintemillas-Verdaguer, M. Montero, C. Serna, A. Roig, L. Casas, B. Martinez and F. Sandiumenge, *Chem. Mater.*, 1999, **11**, 3058-3064.
8. I. Yamashita, *Thin Solid Films*, 2001, **393**, 12-18.
9. J. Liu, C. Huang and Q. He, *Sci. Adv. Mater.*, 2015, **7**, 672-685.

10. J. Ouyang, J. Pei, Q. Kuang, Z. Xie and L. Zheng, *ACS Appl. Mater. Interfaces*, 2014, **6**, 12505-12514.

11. X. Cheng, J. Jiang, D. Jiang and Z. Zhao, *J. Phys. Chem. C*, 2014, **118**, 12588-12598.

12. A. H. Lu, E. L. Salabas and F. Schüth, *Angew. Chem. Int. Edit.*, 2007, **46**, 1222-1244.

13. C. Yang, J. Wu and Y. Hou, *Chem. Commun.*, 2011, **47**, 5130-5141.

14. W. Wu, X. Xiao, F. Ren, S. Zhang and C. Jiang, *J. Low Temp. Phys.*, 2012, **168**, 306-313.

15. L. Liu, H. Z. Kou, W. Mo, H. Liu and Y. Wang, *J. Phys. Chem. B*, 2006, **110**, 15218-15223.

16. J. Xie, K. Chen, H.-Y. Lee, C. Xu, A. R. Hsu, S. Peng, X. Chen and S. Sun, *J. Am. Chem. Soc.*, 2008, **130**, 7542-7543.

17. X. Gou, G. Wang, J. Park, H. Liu and J. Yang, *Nanotechnology*, 2008, **19**, 125606.

18. A. P. Alivisatos, *J. Phys. Chem.*, 1996, **100**, 13226-13239.

19. M. Nirmal and L. Brus, *Acc. Chem. Res.*, 1999, **32**, 407-414.

20. L. Signorini, L. Pasquini, L. Savini, R. Carboni, F. Boscherini, E. Bonetti, A. Giglia, M. Pedio, N. Mahne and S. Nannarone, *Phys. Rev. B*, 2003, **68**, 195423.

21. D. L. Klein, P. L. McEuen, J. E. B. Katari, R. Roth and A. P. Alivisatos, *Appl. Phys. Lett.*, 1996, **68**, 2574-2576.

22. L. Gao, J. Zhuang, L. Nie, J. Zhang, Y. Zhang, N. Gu, T. Wang, J. Feng, D. Yang and S. Perrett, *Nat. Nanotechnol.*, 2007, **2**, 577-583.

23. L. Zhang, H. B. Wu, S. Madhavi, H. H. Hng and X. W. Lou, *J. Am. Chem. Soc.*, 2012, **134**, 17388-17391.

24. B. Wang, J. S. Chen, H. B. Wu, Z. Wang and X. W. Lou, *J. Am. Chem. Soc.*, 2011, **133**, 17146-17148.

25. J. Zhu, Z. Yin, D. Yang, T. Sun, H. Yu, H. E. Hoster, H. H. Hng, H. Zhang and Q. Yan, *Energy Environ. Sci.*, 2013, **6**, 987-993.

26. P. Li, P. Chevallier, P. Ramrup, D. Biswas, D. Vuckovich, M.-A. Fortin and J. K. Oh, *Chem. Mater.*, 2015, **27**, 7100-7109.

27. S. K. Mohapatra, S. E. John, S. Banerjee and M. Misra, *Chem. Mater.*, 2009, **21**, 3048-3055.

28. F. Iskandar, A. Asbahri, E. Dwinanto and M. Abdullah, *Adv. Mater. Res.*, 2015, **1112**, 205-208.

29. V. Patsula, L. Kosinová, M. Lovrić, L. Ferhatovic Hamzić, M. Rabyk, R. Konefal, A. Paruzel, M. Šlouf, V. Herynek and S. k. Gajović, *ACS Appl. Mater. Interfaces*, 2016, **8**, 7238-7247.

30. S. Laurent, D. Forge, M. Port, A. Roch, C. Robic, L. Vander Elst and R. N. Muller, *Chem. Rev.*, 2008, **108**, 2064-2110.

31. S. Sun and H. Zeng, *J. Am. Chem. Soc.*, 2002, **124**, 8204-8205.

32. Z. Li, B. Tan, M. Allix, A. I. Cooper and M. J. Rosseinsky, *Small*, 2008, **4**, 231-239.

33. J. Zhu, K. S. Ng and D. Deng, *Cryst.Growth Des.*, 2014, **14**, 2811-2817.

34. J. Liu, S. Yang, W. Wu, Q. Tian, S. Cui, Z. Dai, F. Ren, X. Xiao and C. Jiang, *ACS Sustainable Chem. Eng.*, 2015, **3**, 2975-2984.

35. A. Shavel and L. M. Liz-Marzán, *Phys. Chem. Chem. Phys.*, 2009, **11**, 3762-3766.

36. W. Wu, S. Yang, J. Pan, L. Sun, J. Zhou, Z. Dai, X. Xiao, H. Zhang and C. Jiang, *CrystEngComm*, 2014, **16**, 5566-5572.

37. B. Geng, J. Ma and J. You, *Cryst. Growth Des.*, 2008, **8**, 1443-1447.

38. H. Hiramatsu and F. E. Osterloh, *Chem. Mater.*, 2004, **16**, 2509-2511.

39. Y. Xia, X. Xia and H. Peng, *J. Am. Chem. Soc.*, 2015, **137**, 7947-7966.

40. Y. Xia, P. Yang, Y. Sun, Y. Wu, B. Mayers, B. Gates, Y. Yin, F. Kim and H. Yan, *Adv. Mater.*, 2003, **15**, 353-389.

41. J. Zhang, X. Liu, L. Wang, T. Yang, X. Guo, S. Wu, S. Wang and S. Zhang, *Nanotechnology*, 2011, **22**, 185501.

42. Y. Ke, Y. Zeng, X. Pu, X. Wu, L. Li, Z. Zhu and Y. Yu, *RSC Adv.*, 2012, **2**, 5676-5682.

43. W. Zhang, X. Wu, J. Hu, Y. Guo and L. Wan, *Adv. Funct. Mater.*, 2008, **18**, 3941-3946.

44. L. Sun, W. Wu, Q. Tian, M. Lei, J. Liu, X. Xiao, X. Zheng, F. Ren and C. Jiang, *ACS Sustainable Chem. Eng.*, 2016, **4**, 1521-1530.

45. C. Jia, L. Sun, Z. Yan, L. You, F. Luo, X. Han, Y. Pang, Z. Zhang and C. Yan, *Angew. Chem.*, 2005, **117**, 4402-4407.

46. T. P. Almeida, M. Fay, Y. Zhu and P. D. Brown, *J. Phys. Chem*, 2009, **100**, 18689-18698.

47. S. Mitra, S. Das, K. Mandal and S. Chaudhuri, *Nanotechnology*, 2007, **18**, 275608.

48. R. Rajendran, R. Muralidharan, R. Santhana Gopalakrishnan, M. Chellamuthu, S. U. Ponnusamy and E. Manikandan, *Eur. J. Inorg. Chem.*, 2011, **2011**, 5384-5389.

49. X. Wang, X. Chen, L. Gao, H. Zheng, M. Ji, C. Tang, T. Shen and Z. Zhang, *J. Mater. Chem.*, 2004, **14**, 905-907.

50. H. Liu, G. Wang, J. Park, J. Wang, H. Liu and C. Zhang, *Electrochim. Acta* 2009, **54**, 1733-1736.

51. Z. Zhong, J. Ho, J. Teo, S. Shen and A. Gedanken, *Chem. Mater.*, 2007, **19**, 4776-4782.

52. H. Sun, B. Chen, X. Jiao, Z. Jiang, Z. Qin and D. Chen, *J. Phys. Chem. C*, 2012, **116**, 5476-5481.

53. Y. Lin, P. R. Abel, A. Heller and C. B. Mullins, *J. Phys. Chem. Lett.*, 2011, **2**, 2885-2891.

54. Z. Li, X. Lai, H. Wang, D. Mao, C. Xing and D. Wang, *Nanotechnology*, 2009, **20**, 245603.

55. L. Zhu, H. Xiao and S. Fu, *Cryst. Growth Des.*, 2007, **7**, 177-182.

56. G. Wang, X. Gou, J. Horvat and J. Park, *J. Phys. Chem. C*, 2008, **112**, 15220-15225.

57. H. Liu, D. Wexler and G. Wang, *J. Alloy Compd.*, 2009, **487**, L24-L27.

58. Y. W. Jun, J. S. Choi and J. Cheon, *Angew. Chem. Int. Edit.*, 2006, **45**, 3414-3439.

59. Z. R. Tian, J. A. Voigt, J. Liu, B. McKenzie, M. J. McDermott, M. A. Rodriguez, H. Konishi and H. Xu, *Nat. Mater.*, 2003, **2**, 821-826.

60. J. Qu, Y. Yu, C. Y. Cao and W. G. Song, *Chem. Eur.-J.*, 2013, **19**, 11172-11177.

61. X. Li, Z. Si, Y. Lei, J. Tang, S. Wang, S. Su, S. Song, L. Zhao and H. Zhang, *CrystEngComm*, 2010, **12**, 2060-2063.

62. J. Wu, H. Zhang, N. Du, X. Ma and D. Yang, *J. Phys. Chem. B*, 2006, **110**, 11196-11198.

63. L. Wang, T. Fei, Z. Lou and T. Zhang, *ACS Appl. Mater. Interfaces*, 2011, **3**, 4689-4694.

64. J. Liang, L. Li and H. Kang, *Powder Technol.*, 2013, **235**, 475-478.

65. F. Song, J. Guan, X. Fan and G. Yan, *J. Alloy Compd.*, 2009, **485**, 753-758.

66. N. Bao, L. Shen, W. An, P. Padhan, C. Heath Turner and A. Gupta, *Chem. Mater.*, 2009, **21**, 3458-3468.

67. M. Cao, T. Liu, S. Gao, G. Sun, X. Wu, C. Hu and Z. L. Wang, *Angew. Chem. Int. Edit.*, 2005, **44**, 4197-4201.

68. Y. S. Cho and Y. D. Huh, *Bull. Korean. Chem. Soc.*, 2009, **30**, 1413-1415.

69. X. Zhang, C. Sui, J. Gong, Z. Su and L. Qu, *J. Phys. Chem. C*, 2007, **111**, 9049-9054.

70. S. H. Lee, Y. Song, I. D. Hosein and C. M. Liddell, *J. Mater. Chem.*, 2009, **19**, 350-355.

71. Z. An, J. Zhang, S. Pan and G. Song, *Powder Technol.*, 2012, **217**, 274-280.

72. F. L. Souza, K. P. Lopes, P. A. Nascente and E. R. Leite, *Sol. Energy Mater. Sol. Cells*, 2009, **93**, 362-368.

73. G. Tong, J. Guan, W. Wu, L. Li, Y. Guan and Q. Hua, *Sci. China Technol. Sci.*, 2010, **53**, 1897-1903.

74. S. Li, H. Zhang, J. Wu, X. Ma and D. Yang, *Cryst. Growth Des.*, 2006, **6**, 351-353.

75. C. Hao, Y. Shen, Z. Wang, X. Wang, F. Feng, C. Ge, Y. Zhao and K. Wang, *ACS Sustainable Chem. Eng.*, 2016, **4**, 1069-1077.

76. D. Amara, J. Grinblat and S. Margel, *J. Mater. Chem.*, 2012, **22**, 2188-2195.

77. X. Wang, Z. Zhao, J. Qu, Z. Wang and J. Qiu, *Cryst. Growth Des.*, 2010, **10**, 2863-2869.

78. M. P. Kapoor, S. Inagaki, S. Ikeda, K. Kakiuchi, M. Suda and T. Shimada, *J. Am. Chem. Soc.*, 2005, **127**, 8174-8178.

79. W. Xiong and J. Peng, *Water Res.*, 2008, **42**, 4869-4877.

80. M. Zhu and G. Diao, *J. Phys. Chem. C*, 2011, **115**, 18923-18934.

81. Y. Zheng, Y. Cheng, Y. Wang, F. Bao, L. Zhou, X. Wei, Y. Zhang and Q. Zheng, *J. Phys. Chem. B*, 2006, **110**, 3093-3097.

82. L. Zhang, H. B. Wu, R. Xu and X. W. D. Lou, *CrystEngComm*, 2013, **15**, 9332-9335.

83. S. Yuan, Z. Zhou and G. Li, *CrystEngComm*, 2011, **13**, 4709-4713.

84. X. Xu, R. Cao, S. Jeong and J. Cho, *Nano Lett.*, 2012, **12**, 4988-4991.

85. F. Dong, W. Guo and C.-S. Ha, *J. Nanopart. Res.*, 2012, **14**, 1-8.

86. J. Lian, X. Duan, J. Ma, P. Peng, T. Kim and W. Zheng, *ACS Nano*, 2009, **3**, 3749-3761.

87. W. Wu, S. Zhang, X. Xiao, J. Zhou, F. Ren, L. Sun and C. Jiang, *ACS Appl. Mater. Interfaces*, 2012, **4**, 3602-3609.

88. Z. Xiao, Y. Xia, Z. Ren, Z. Liu, G. Xu, C. Chao, X. Li, G. Shen and G. Han, *J. Mater. Chem.*, 2012, **22**, 20566-20573.

89. J. Xu and Y. Zhu, *ACS Appl. Mater. Interfaces*, 2012, **4**, 4752-4757.

90. S. Xuan, F. Wang, J. M. Lai, K. W. Sham, Y. X. J. Wang, S. F. Lee, J. C. Yu, C. H. Cheng and K. C. F. Leung, *ACS Appl. Mater. Interfaces*, 2011, **3**, 237-244.

91. S. Zhang, W. Wu, X. Xiao, J. Zhou, F. Ren and C. Jiang, *Nanoscale Res. Lett.*, 2011, **6**, 1-9.

92. L. Liu, X. Yang, C. Lv, A. Zhu, X. Zhu, S. Guo, C. Chen and D. Yang, *ACS Appl. Mater. Interfaces*, 2016, **8**, 7047-7053.

93. S. Cao and Y. Zhu, *J. Phys. Chem. C*, 2008, **112**, 6253-6257.

94. W. Zhao, H. Chen, Y. Li, L. Li, M. Lang and J. Shi, *Adv. Funct. Mater.*, 2008, **18**, 2780-2788.

95. H. Song, X. Jia, H. Qi, X. Yang, H. Tang and C. Min, *J. Mater. Chem.*, 2012, **22**, 3508-3516.

96. W. Wu, X. Xiao, S. Zhang, H. Li, X. Zhou and C. Jiang, *Nanoscale Res. Lett.* , 2009, **4**, 926-931.

97. A. Cabot, V. F. Puntes, E. Shevchenko, Y. Yin, L. Balcells, M. A. Marcus, S. M. Hughes and A. P. Alivisatos, *J. Am. Chem. Soc.*, 2007, **129**, 10358-10360.

98. B. Koo, H. Xiong, M. D. Slater, V. B. Prakapenka, M. Balasubramanian, P. Podsiadlo, C. S. Johnson, T. Rajh and E. V. Shevchenko, *Nano Lett.*, 2012, **12**, 2429-2435.

99. K. Cheng, S. Peng, C. Xu and S. Sun, *J. Am. Chem. Soc.*, 2009, **131**, 10637-10644.

100. Z. Wang, L. Wu, M. Chen and S. Zhou, *J. Am. Chem. Soc.* , 2009, **131**, 11276-11277.

101. F. Zhang, H. Yang, X. Xie, L. Li, L. Zhang, J. Yu, H. Zhao and B. Liu, *Sens. Actuators B: Chem.*, 2009, **141**, 381-389.

102. J. Yu, X. Yu, B. Huang, X. Zhang and Y. Dai, *Cryst. Growth Des.*, 2009, **9**, 1474-1480.

103. X. Liu, Y. Li, W. Zhu and P. Fu, *CrystEngComm*, 2013, **15**, 4937-4947.

104. S. Iijima, *Nature*, 1991, **354**, 56-58.

105. J. Escrig, J. Bachmann, J. Jing, M. Daub, D. Altbir and K. Nielsch, *Phys. Rev. B*, 2008, **77**, 214421.

106. J. Sundaramurthy, P. S. Kumar, M. Kalaivani, V. Thavasi, S. G. Mhaisalkar and S. Ramakrishna, *RSC Adv.*, 2012, **2**, 8201-8208.

107. R. Yuan, X. Fu, X. Wang, P. Liu, L. Wu, Y. Xu, X. Wang and Z. Wang, *Chem. Mater.*, 2006, **18**, 4700-4705.

108. S. Zeng, K. Tang, T. Li, Z. Liang, D. Wang, Y. Wang and W. Zhou, *J. Phys. Chem. C*, 2007, **111**, 10217-10225.

109. X. Li, X. Yu, J. He and Z. Xu, *J. Phys. Chem. C*, 2009, **113**, 2837-2845.

110. J. Liu, W. Wu, Q. Tian, S. Yang, L. Sun, X. Xiao, F. Ren, C. Jiang and V. A. Roy, *RSC Adv.*, 2015, **5**, 61239-61248.

111. Z. Sun, H. Yuan, Z. Liu, B. Han and X. Zhang, *Adv. Mater.*, 2005, **17**, 2993-2997.

112. X. Hu, J. C. Yu, J. Gong, Q. Li and G. Li, *Adv. Mater.*, 2007, **19**, 2324-2329.

113. X. Zhang, M. Tsuji, S. Lim, N. Miyamae, M. Nishio, S. Hikino and M. Umezu, *Langmuir*, 2007, **23**, 6372-6376.

114. H. Fan, J. Yi, Y. Yang, K. W. Kho, H. Tan, Z. X. Shen, J. Ding, X. Sun, M. C. Olivo and Y. Feng, *ACS Nano*, 2009, **3**, 2798-2808.

115. H. Fan, G. You, Y. Li, Z. Zheng, H. Tan, Z. Shen, S. Tang and Y. Feng, *J. Phys. Chem. C*, 2009, **113**, 9928-9935.

116. B. Tao, Q. Zhang, Z. Liu and B. Geng, *Mater. Chem. Phys.*, 2012, **136**, 604-612.

117. H. Xu, H. Bi and R. Yang, *J. Appl. Phys.*, 2012, **111**, 07A522.

118. Y. Wang, Q. Li, L. Yu, J. Travas-Sejdic and L. Zhang, *Chinese J. Polym. Sci.*, 2013, **31**, 503-513.

119. J. Zou, Z. Wang, M. Yan and H. Bi, *J. Phys. D: Appl. Phys.*, 2014, **47**, 275001.

120. Y. Liu, C. Yu, W. Dai, X. Gao, H. Qian, Y. Hu and X. Hu, *J. Alloy Compd.*, 2013, **551**, 440-443.

121. B. Lv, Y. Xu, D. Wu and Y. Sun, *Chem. Commun.*, 2011, **47**, 967-969.

122. R. M. Cornell and U. Schwertmann, *The iron oxides: structure, properties, reactions, occurrences and uses*, John Wiley & Sons, 2003.

123. W. Wu, C. Z. Jiang and V. A. L. Roy, *Nanoscale*, 2015, **7**, 38-58.

124. A. Demortiere, P. Panissod, B. Pichon, G. Pourroy, D. Guillon, B. Donnio and S. Begin-Colin, *Nanoscale*, 2011, **3**, 225-232.

125. M. Yamaura, R. Camilo, L. Sampaio, M. Macedo, M. Nakamura and H. Toma, *J. Magn. Magn. Mater.*, 2004, **279**, 210-217.

126. G. Herzer, *IEEE Trans. Magn.*, 1990, **26**, 1397-1402.

127. G. Herzer, *J. Magn. Magn. Mater.*, 1992, **112**, 258-262.

128. M. Ma, Y. Wu, J. Zhou, Y. Sun, Y. Zhang and N. Gu, *J. Magn. Magn. Mater.*, 2004, **268**, 33-39.

129. J. Choi, J. Cha and J.-K. Lee, *RSC Adv.*, 2013, **3**, 8365-8371.

130. W. Wu, X. Xiao, F. Ren, S. Zhang and C. Jiang, *J. Low Temp. Phys.*, 2012, **168**, 306-313.

131. H. Sun, H. Shi, F. Zhao, L. Qi and S. Gao, *Chem. Commun.*, 2005, **34**, 4339-4341.

132. S. Bharathi, D. Nataraj, M. Seetha, D. Mangalaraj, N. Ponpandian, Y. Masuda, K. Senthil and K. Yong, *CrystEngComm*, 2010, **12**, 373-382.

133. Q. Gao, X. Wang, J. Di, X. Wu and Y. Tao, *Catal. Sci. Technol.*, 2011, **1**, 574-577.

134. G. Qiu, H. Huang, H. Genuino, N. Opembe, L. Stafford, S. Dharmarathna and S. L. Suib, *J. Phys. Chem. C*, 2011, **115**, 19626-19631.

135. B. Reddy, F. Rasouli, M. Hajaligol and S. Khanna, *Fuel*, 2004, **83**, 1537-1541.

136. X. Mou, X. Wei, Y. Li and W. Shen, *CrystEngComm*, 2012, **14**, 5107-5120.

137. Y. Zhao, F. Pan, H. Li, T. Niu, G. Xu and W. Chen, *J. Mater. Chem. A*, 2013, **1**, 7242-7246.

138. A. Kanazawa, S. Kanaoka and S. Aoshima, *J. Am. Chem. Soc.,* 2007, **129**, 2420-2421.

139. W. Zhang, J. Chen, X. Wang, H. Qi and K. Peng, *Appl. Organomet. Chem.*, 2009, **23**, 200-203.

140. A. Tricoli, M. Righettoni and A. Teleki, *Angew. Chem. Int. Edit.*, 2010, **49**, 7632-7659.

141. N. Barsan and U. Weimar, *J. Electroceram.*, 2001, **7**, 143-167.

142. D. Kohl, *Sens. Actuators*, 1989, **18**, 71-113.

143. Y. Liu, Y. Jiao, Z. Zhang, F. Qu, A. Umar and X. Wu, *ACS Appl. Mater. Interfaces*, 2014, **6**, 2174-2184.

144. Z. Jing and J. Zhan, *Adv. Mater.*, 2008, **20**, 4547-4551.

145. S. Bai, K. Zhang, R. Luo, D. Li, A. Chen and C. C. Liu, *J. Mater. Chem.*, 2012, **22**, 12643-12650.

146. P. Gunawan, L. Mei, J. Teo, J. Ma, J. Highfield, Q. Li and Z. Zhong, *Langmuir*, 2012, **28**, 14090-14099.

147. Z. Zhong, J. Highfield, M. Lin, J. Teo and Y.-f. Han, *Langmuir*, 2008, **24**, 8576-8582.

148. Z. Tianshu, P. Hing and Z. Ruifang, *J. Mater. Sci.*, 2000, **35**, 1419-1425.

149. P. Guo, L. Cui, Y. Wang, M. Lv, B. Wang and X. Zhao, *Langmuir*, 2013, **29**, 8997-9003.

150. Z. Ai, K. Deng, Q. Wan, L. Zhang and S. Lee, *The J. Phys. Chem. C*, 2010, **114**, 6237-6242.

151. X. Rao, X. Su, C. Yang, J. Wang, X. Zhen and D. Ling, *CrystEngComm*, 2013, **15**, 7250-7256.

152. J. Ouyang, J. Pei, Q. Kuang, Z. Xie and L. Zheng, *ACS Appl. Mater. Interfaces*, 2014, **6**, 12505-12514.

153. Y. Yang, H. Ma, J. Zhuang and X. Wang, *Inorg. Chem.*, 2011, **50**, 10143-10151.

154. H. Song, X. Jia and X. Zhang, *J. Mater. Chem.*, 2012, **22**, 22699-22705.

155. Y. Kang, S. Risbud, J. F. Rabolt and P. Stroeve, *Chem. Mater.*, 1996, **8**, 2209-2211.

156. J. Lee, T. Isobe and M. Senna, *Colloids Surf. A*, 1996, **109**, 121-127.

157. M. Salavati-Niasari, T. Mahmoudi and O. Amiri, *J. Clust. Sci.*, 2012, **23**, 597-602.

158. J. Rockenberger, E. C. Scher and A. P. Alivisatos, *J. Am. Chem. Soc.*, 1999, **121**, 11595-11596.

159. D. Farrell, S. A. Majetich and J. P. Wilcoxon, *J. Phys. Chem. B*, 2003, **107**, 11022-11030.

160. K. Woo, J. Hong, S. Choi, H. W. Lee, J. P. Ahn, C. S. Kim and S. W. Lee, *Chem. Mater.*, 2004, **16**, 2814-2818.

161. J. Park, J. Joo, S. G. Kwon, Y. Jang and T. Hyeon, *Angew. Chem. Int. Edit.*, 2007, **46**, 4630-4660.

162. J. Park, K. An, Y. Hwang, J. G. Park, H. J. Noh, J. Y. Kim, J. H. Park, N. M. Hwang and T. Hyeon, *Nat. Mater.*, 2004, **3**, 891-895.

163. M. V. Kovalenko, M. I. Bodnarchuk, R. T. Lechner, G. Hesser, F. Schäffler and W. Heiss, *J. Am. Chem. Soc.*, 2007, **129**, 6352-6353.

164. J. Ma, J. Lian, X. Duan, X. Liu and W. Zheng, *J. Phys. Chem. C*, 2010, **114**, 10671-10676.

165. X. Sun, C. Zheng, F. Zhang, Y. Yang, G. Wu, A. Yu and N. Guan, *J. Phys. Chem. C*, 2009, **113**, 16002-16008.

166. H. Zhu, D. Yang, L. Zhu, H. Yang, D. Jin and K. Yao, *J. Mater. Sci.*, 2007, **42**, 9205-9209.

167. F. Jiao, J. C. Jumas, M. Womes, A. V. Chadwick, A. Harrison and P. G. Bruce, *J. Am. Chem. Soc.*, 2006, **128**, 12905-12909.

168. W. Wu, X. Xiao, S. Zhang, J. Zhou, L. Fan, F. Ren and C. Jiang, *J. Phys. Chem. C*, 2010, **114**, 16092-16103.

169. Q. Tian, W. Wu, L. Sun, S. Yang, M. Lei, J. Zhou, Y. Liu, X. Xiao, F. Ren and C. Jiang, *ACS Appl. Mater. Interfaces*, 2014, **6**, 13088-13097.

170. E. E. Carpenter, C. T. Seip and C. J. O'Connor, *J. Appl. Phys.*, 1999, **85**, 5184-5186.

171. A. K. Gupta and M. Gupta, *Biomaterials*, 2005, **26**, 3995-4021.

172. M. Darbandi, F. Stromberg, J. Landers, N. Reckers, B. Sanyal, W. Keune and H. Wende, *J. Phys. D: Appl. Phys.*, 2012, **45**, 195001.

173. Y. Zhao, L. N. Lin, Y. Lu, H. L. Gao, S. F. Chen, P. Yang and S. H. Yu, *Adv. Healthc. Mater.*, 2012, **1**, 327-331.

174. Z. Wu, S. Yang and W. Wu, *Nanoscale*, 2016, **8**, 1237-1259.

175. L. Ratke and P. W. Voorhees, *Growth and coarsening: Ostwald ripening in material processing*, Springer, 2002.

176. W. Ostwald, *Lehrbuch der allgemeinen Chemie*, W. Engelmann, 1886.

177. P. Somasundaran, *Encyclopedia of surface and colloid science*, CRC Press, 2006.

178. H. ChunáZeng, *J. Mater. Chem. A*, 2014, **2**, 4843-4851.

179. V. Burlakov, *arXiv preprint arXiv:0710.5224*, 2007.

180. P. W. Voorhees, *J. Stat. Phys.*, 1985, **38**, 231-252.

181. D. Deng, S. T. Martin and S. Ramanathan, *J. Mater. Res.*, 2011, **26**, 1545-1551.

182. C. C. Yec and H. Zeng, *J. Mater. Chem. A*, 2014, **2**, 4843-4851.

183. J. Ma, T. Wang, X. Duan, J. Lian, Z. Liu and W. Zheng, *Nanoscale*, 2011, **3**, 4372-4375.

184. J. Zhu, K. S. Ng and D. Deng, *ACS Appl. Mater. Interfaces*, 2014, **6**, 2996-3001.

185. M. Lin, H. R. Tan, J. P. Y. Tan and S. Bai, *J. Phys. Chem. C*, 2013, **117**, 11242-11250.

186. R. L. Penn and J. F. Banfield, *Science*, 1998, **281**, 969-971.

187. R. L. Penn and J. F. Banfield, *Am. Mineral.*, 1998, **83**, 1077-1082.

188. Q. Zhang, S. Liu and S. Yu, *J. Mater. Chem.*, 2009, **19**, 191-207.

189. A. Alivisatos, *Science*, 2000, **289**, 736-737.

190. D. Li, M. H. Nielsen, J. R. Lee, C. Frandsen, J. F. Banfield and J. J. De Yoreo, *Science*, 2012, **336**, 1014-1018.

191. J. F. Banfield, S. A. Welch, H. Zhang, T. T. Ebert and R. L. Penn, *Science*, 2000, **289**, 751-754.

192. E. J. Lee, C. Ribeiro, E. Longo and E. R. Leite, *J. Phys. Chem. B*, 2005, **109**, 20842-20846.

193. J. K. Bailey, C. J. Brinker and M. L. Mecartney, *J. Colloid Interface Sci.*, 1993, **157**, 1-13.

194. M. Ocana, M. P. Morales and C. J. Serna, *J. Colloid Interface Sci.*, 1995, **171**, 85-91.

195. Y. Zhu, W. Zhao, H. Chen and J. Shi, *J. Phys. Chem. C*, 2007, **111**, 5281-5285.

196. B. Cheng, J. M. Russell, W. Shi, L. Zhang and E. T. Samulski, *J. Am. Chem. Soc.*, 2004, **126**, 5972-5973.

197. M. Adachi, Y. Murata, J. Takao, J. Jiu, M. Sakamoto and F. Wang, *J. Am. Chem. Soc.*, 2004, **126**, 14943-14949.

198. J. Zhang, F. Huang and Z. Lin, *Nanoscale*, 2010, **2**, 18-34.

199. Y. W. Jun, M. F. Casula, J. H. Sim, S. Y. Kim, J. Cheon and A. P. Alivisatos, *J. Am. Chem. Soc.*, 2003, **125**, 15981-15985.

200. K. S. Cho, D. V. Talapin, W. Gaschler and C. B. Murray, *J. Am. Chem. Soc.*, 2005, **127**, 7140-7147.

201. Y. Guyodo, A. Mostrom, R. Lee Penn and S. K. Banerjee, *Geophys. Res. Lett.*, 2003, **30**, 1512.

202. D. J. Burleson and R. L. Penn, *Langmuir*, 2006, **22**, 402-409.

203. X. Li, W. Wei, S. Wang, L. Kuai and B. Geng, *Nanoscale*, 2011, **3**, 718-724.

204. X. Lai, J. E. Halpert and D. Wang, *Energy Environ. Sci.*, 2012, **5**, 5604-5618.

205. B. Jia and L. Gao, *Cryst. Growth Des.*, 2008, **8**, 1372-1376.

206. H. Zhang, F. Huang, B. Gilbert and J. F. Banfield, *J. Phys. Chem. B*, 2003, **107**, 13051-13060.

207. H. Guo and A. S. Barnard, *J. Colloid Interface Sci.*, 2012, **386**, 315-324.

208. J. W. Seo, Y. W. Jun, S. J. Ko and J. Cheon, *J. Phys. Chem. B*, 2005, **109**, 5389-5391.

209. Z. Zhang, X. Zhong, S. Liu, D. Li and M. Han, *Angew. Chem.*, 2005, **117**, 3532-3536.

210. Z. Liu, B. Lv, Y. Xu and D. Wu, *J. Mater. Chem. A*, 2013, **1**, 3040-3046.

211. B. Lv, Y. Xu, D. Wu and Y. Sun, *CrystEngComm*, 2011, **13**, 7293-7298.

212. B. Lv, Z. Liu, H. Tian, Y. Xu, D. Wu and Y. Sun, *Adv. Funct. Mater.*, 2010, **20**, 3987-3996.

213. W. Li, B. Lv and Y. Xu, *J. Nanopart. Res.*, 2013, **15**, 1-9.

214. Y. Zeng, R. Hao, B. Xing, Y. Hou and Z. Xu, *Chem. Commun.*, 2010, **46**, 3920-3922.

215. D. Zhang, X. Zhang, X. Ni, J. Song and H. Zheng, *Cryst. Growth Des.*, 2007, **7**, 2117-2119.

216. X. Hu and J. C. Yu, *Adv. Funct. Mater.*, 2008, **18**, 880-887.

217. A. Smigelskas and E. Kirkendall, *Trans. Aime*, 1947, **171**, 130-142.

218. Y. Yin, R. M. Rioux, C. K. Erdonmez, S. Hughes, G. A. Somorjai and A. P. Alivisatos, *Science*, 2004, **304**, 711-714.

219. P. Chernavskii, G. Pankina, V. Zaikovskii, N. Peskov and P. Afanasiev, *J. Phys. Chem. C*, 2008, **112**, 9573-9578.

220. P. Y. Keng, B. Y. Kim, I. B. Shim, R. Sahoo, P. E. Veneman, N. R. Armstrong, H. Yoo, J. E. Pemberton, M. M. Bull and J. J. Griebel, *ACS Nano*, 2009, **3**, 3143-3157.

221. Y. Yin, C. K. Erdonmez, A. Cabot, S. Hughes and A. P. Alivisatos, *Adv. Funct. Mater.*, 2006, **16**, 1389-1399.

222. Q. Peng, X. Sun, J. C. Spagnola, C. Saquing, S. A. Khan, R. J. Spontak and G. N. Parsons, *ACS Nano*, 2009, **3**, 546-554.

223. A. Cabot, M. Ibánez, P. Guardia and A. P. Alivisatos, *J. Am. Chem. Soc.*, 2009, **131**, 11326-11328.

224. W. Pan, J. W. Ye, G. L. Ning, Y. Lin and J. Wang, *Mater. Res. Bull.*, 2009, **44**, 280-283.

225. J. G. Railsback, A. C. Johnston-Peck, J. Wang and J. B. Tracy, *ACS Nano*, 2010, **4**, 1913-1920.

226. G. Leibbrandt, G. Hoogers and F. Habraken, *Phys. Rev. Lett.*, 1992, **68**, 1947.

227. C. Jimmy and C. WanáLeung, *Chem. Commun.*, 2005, 2683-2685.

228. Q. Wang, B. Geng, S. Wang, Y. Ye and B. Tao, *Chem. Commun.*, 2010, **46**, 1899-1901.

229. J. H. Fendler, *Chem. Mater.*, 1996, **8**, 1616-1624.

230. G. Whitesides, J. Mathias and C. Seto, *Science*, 1991, **254**, 1312-1319.

231. G. M. Whitesides and B. Grzybowski, *Science*, 2002, **295**, 2418-2421.

232. J. Chen, M. Shi, P. Liu, A. Ko, W. Zhong, W. Liao and M. M. Xing, *Biomaterials*, 2014, **35**, 1240-1248.

233. S. H. Lee, S. H. Yu, J. E. Lee, A. Jin, D. J. Lee, N. Lee, H. Jo, K. Shin, T. Y. Ahn and Y. W. Kim, *Nano Lett.* , 2013, **13**, 4249-4256.

234. S. Disch, E. Wetterskog, R. P. Hermann, G. Salazar-Alvarez, P. Busch, T. Brückel, L. Bergström and S. Kamali, *Nano Lett.*, 2011, **11**, 1651-1656.

235. L. Zhang, D. L. Sheng, R. Zhang, E. Y. Chu, J. P. Liu and S. L. Zhou, *Applied Mechanics and Materials*, 2014, **446**, 210-213.

236. T. Brezesinski, M. Groenewolt, M. Antonietti and B. Smarsly, *Angew. Chem. Int. Edit.* , 2006, **45**, 781-784.

237. P. N. Nguyen, G. Nikolova, P. Polavarapu, G. Waton, L. T. Phuoc, G. Pourroy and M. P. Krafft, *RSC Adv.*, 2013, **3**, 7743-7746.

238. J. Fei, Y. Cui, J. Zhao, L. Gao, Y. Yang and J. Li, *J. Mater. Chem.* , 2011, **21**, 11742-11746.

239. L. Zhong, J. Hu, H. Liang, A. Cao, W. Song and L. Wan, *Adv. Mater.*, 2006, **18**, 2426-2431.

240. W. Wu, Q. He and C. Jiang, *Nanoscale Res. Lett.*, 2008, **3**, 397-415.

241. T. Hisatomi, J. Kubota and K. Domen, *Chem. Soc. Rev.*, 2014, **43**, 7520-7535.

242. K. Itoh and J. M. Bockris, *J. Appl. Phys.*, 1984, **56**, 874-876.

243. J. Brillet, M. Gratzel and K. Sivula, *Nano Lett.*, 2010, **10**, 4155-4160.

244. B. D. Chernomordik, H. B. Russell, U. Cvelbar, J. B. Jasinski, V. Kumar, T. Deutsch and M. K. Sunkara, *Nanotechnology*, 2012, **23**, 194009.

245. T. J. LaTempa, X. Feng, M. Paulose and C. A. Grimes, *J. Phys. Chem. C*, 2009, **113**, 16293-16298.

246. J. Li, S. K. Cushing, P. Zheng, F. Meng, D. Chu and N. Wu, *Nat. Commun.*, 2013, **4**.

247. Y. Hou, F. Zuo, A. Dagg and P. Feng, *Nano Lett.*, 2012, **12**, 6464-6473.

248. J. S. Jang, J. Lee, H. Ye, F.-R. F. Fan and A. J. Bard, *J. Phys. Chem. C*, 2009, **113**, 6719-6724.

249. I. Cesar, K. Sivula, A. Kay, R. Zboril and M. Grätzel, *J. Phys. Chem. C*, 2008, **113**, 772-782.

250. N. J. Cherepy, D. B. Liston, J. A. Lovejoy, H. Deng and J. Zhang, *J. Phys. Chem. B*, 1998, **102**, 770-776.

251. M. P. Dare-Edwards, J. B. Goodenough, A. Hamnett and P. R. Trevellick, *J. Chem. Soc., Faraday Trans.*, 1983, **79**, 2027-2041.

252. Y.-S. Hu, A. Kleiman-Shwarsctein, A. J. Forman, D. Hazen, J.-N. Park and E. W. McFarland, *Chem. Mater.*, 2008, **20**, 3803-3805.

253. M. Barroso, C. A. Mesa, S. R. Pendlebury, A. J. Cowan, T. Hisatomi, K. Sivula, M. Grätzel, D. R. Klug and J. R. Durrant, *PNAS*, 2012, **109**, 15640-15645.

254. A. Hagfeldt, G. Boschloo, L. Sun, L. Kloo and H. Pettersson, *Chem. Rev.*, 2010, **110**, 6595-6663.

255. M. Grätzel, *J. Photochem. Photobiol., C*, 2003, **4**, 145-153.

256. G. K. Mor, K. Shankar, M. Paulose, O. K. Varghese and C. A. Grimes, *Nano Lett.*, 2006, **6**, 215-218.

257. U. Bach, D. Lupo, P. Comte, J. Moser, F. Weissörtel, J. Salbeck, H. Spreitzer and M. Grätzel, *Nature*, 1998, **395**, 583-585.

258. S. Agarwala, Z. Lim, E. Nicholson and G. Ho, *Nanoscale*, 2012, **4**, 194-205.

259. X. Shang, Z. Guo, W. Gan, R. Zhou, C. Ma, K. Hu, H. Niu and J. Xu, *Ionics*, 2016, **22**, 435-443.

260. H. Niu, S. Zhang, Q. Ma, S. Qin, L. Wan, J. Xu and S. Miao, *RSC Adv.*, 2013, **3**, 17228-17235.

261. A. Manikandan, A. Saravanan, S. A. Antony and M. Bououdina, *J. Nanosci. Nanotechnol.*, 2015, **15**, 4358-4366.

262. M. Wu and T. Ma, *J. Phys. Chem. C*, 2014, **118**, 16727-16742.

263. Y. Hou, D. Wang, X. H. Yang, W. Q. Fang, B. Zhang, H. F. Wang, G. Z. Lu, P. Hu, H. J. Zhao and H. G. Yang, *Nat. Commun.*, 2013, **4**, 1583.

264. W. Wang, X. Pan, W. Liu, B. Zhang, H. Chen, X. Fang, J. Yao and S. Dai, *Chem. Commun.*, 2014, **50**, 2618-2620.

265. W. Yang, X. Xu, Z. Li, F. Yang, L. Zhang, Y. Li, A. Wang and S. Chen, *Carbon*, 2016, **96**, 947-954.

266. M. Shahpari, A. Behjat, M. Khajaminian and N. Torabi, *Sol. Energy*, 2015, **119**, 45-53.

267. B. M. Klahr and T. W. Hamann, *J. Phys. Chem. C*, 2011, **115**, 8393-8399.

268. S. Reda, *Mater. Sci. Semicond. Process.*, 2010, **13**, 417-425.

269. K. Sivula, R. Zboril, F. Le Formal, R. Robert, A. Weidenkaff, J. Tucek, J. Frydrych and M. Gratzel, *J. Am. Chem. Soc.*, 2010, **132**, 7436-7444.

270. B. Kılıç, N. Gedik, S. P. Mucur, A. S. Hergul and E. Gür, *Mater. Sci. Semicond. Process.*, 2015, **31**, 363-371.

271. J. S. Im, S. K. Lee and Y. S. Lee, *Appl. Surf. Sci.*, 2011, **257**, 2164-2169.

272. A. S. Aricò, P. Bruce, B. Scrosati, J.-M. Tarascon and W. Van Schalkwijk, *Nat. Mater.*, 2005, **4**, 366-377.

273. J. Maier, *Nat. Mater.*, 2005, **4**, 805-815.

274. J. M. Jeong, B. G. Choi, S. C. Lee, K. G. Lee, S. J. Chang, Y. K. Han, Y. B. Lee, H. U. Lee, S. Kwon and G. Lee, *Adv. Mater.*, 2013, **25**, 6250-6255.

275. P. Poizot, S. Laruelle, S. Grugeon, L. Dupont and J. Tarascon, *Nature*, 2000, **407**, 496-499.

276. G. Zhou, D. Wang, F. Li, L. Zhang, N. Li, Z. Wu, L. Wen, G. Q. Lu and H. Cheng, *Chem. Mater.*, 2010, **22**, 5306-5313.

277. D. Bresser, E. Paillard, R. Kloepsch, S. Krueger, M. Fiedler, R. Schmitz, D. Baither, M. Winter and S. Passerini, *Adv. Energy Mater.*, 2013, **3**, 513-523.

278. Z. Wu, K. Yu, S. Zhang and Y. Xie, *J. Phys. Chem. C*, 2008, **112**, 11307-11313.

Caption

Figure 1 Typical morphology of solid IONCs with the shapes of 0D, 1D, 2D and other complex structure.

Figure 2 (a) SEM, (b) TEM image (inset: SAED pattern), (c) top-down HRTEM image of a-Fe_2O_3. (reprinted from ref. 60, Copyright (2013) with permission from the John Wiley and Sons) (d) SEM image of Fe_3O_4 triangular nanoprisms. (reprinted from ref. 61, Copyright (2010) with permission from the Royal Society of Chemistry) (e, f)TEM image and SAED pattern of hexagonal Fe_2O_3 nanoplate. (reprinted from ref. 62, Copyright (2006) with permission from the American Chemical Society)

Figure 3. SEM images of Fe_3O_4 prepared in different solvents without additive at 350 °C for 6 h, (a) IPA; (b) IPA/water at 8:1; (c) IPA/water at 5:1; (d) pure water. (reprinted from ref. 77, Copyright (2010) with permission from the American Chemical Society)

Figure 4 Typical morphology of mesoporous IONCs.

Figure 5 (a) Fabrication of mesoporous Fe_3O_4 nano/microspheres with large surface area, (b-e) TEM image of corresponding product for each synthesis process of mesoporous Fe_3O_4 microspheres by template method. (reprinted from ref. 90, Copyright (2011) with permission from the American Chemical Society) (f, g) SEM and TEM images of α-Fe_2O_3 nanospindles, (h, i) SEM and TEM images of mesoporous Fe_3O_4 nanospindles obtained by reduction of α-Fe_2O_3 nanospindles.

Figure 6 Typical morphology of hollow IONCs.

Figure 7 (a) Formation process and corresponding SEM images of cage-like Fe_2O_3 hollow sphere, (b-e) SEM images of corresponding product for each synthesis process of cage-like Fe_2O_3 hollow sphere. (reprinted from ref. 102, Copyright (2009) with permission from the American Chemical Society) (f) Formation mechanism of porous Fe_3O_4 hollow nanospheres, (g) SEM and inset TEM images of hollow Fe_3O_4 NPs through solvothermal method. (reprinted from ref. 103, Copyright (2013) with permission

from the Royal Society of Chemistry)

Figure 8 (a) The formation process of the hexagonal inner ring, (b) experimental and crystal structural evolution of the hexagonal inner ring. (reprinted from ref. 121, Copyright (2011) with permission from the Royal Society of Chemistry)

Figure 9 Schematic presentation of classification of magnetism (a) and the typical hysteresis loops of magnetic iron oxide NPs (b): superparamagnetic ferrites (curve a), soft ferrites (curve b), hard ferrites (curve c).

Figure 10 Room temperature magnetic hysteresis loops of nanostructured α-Fe_2O_3 with (a) dendritic, (b) single layered snowflake, and (c) double-layered snowflake morphology. The inset images are the corresponding magnified hysteresis loops and microstructure for each sample. (reprinted from ref. 132, Copyright (2010) with permission from the Royal Society of Chemistry)

Figure 11 TEM images of monodisperse spherical (a-c), cubic (d-f) and bipyramidal (g) Fe_3O_4 NCs with different particle sizes. These Fe_3O_4 NCs with different morphologies are obtained by changing the stabilizer and their ratio of oleate/$Fe(OL)_3$. Fe_3O_4 NCs with different sizes are obtained by changing the temperature. (reprinted from ref. 163, Copyright (2007) with permission from the American Chemical Society)

Figure 12 Schematic illustration of the shape evolution for hematite nanostructures at different reaction times and different ferric concentrations. (reprinted from ref. 168, Copyright (2010) with permission from the American Chemical Society)

Figure 13 (a) Illustration of the proposed formation mechanism for hollow nanococoons; (b) *ex situ* electron microscope images for samples prepared from 15, 30, 75 min, and 3 h. (reprinted from ref. 184, Copyright (2014) with permission from the American Chemical Society)

Figure 14 (a) Schematic illustration of the formation mechanism and (b) corresponding TEM and SEM images of cubic α-Fe_2O_3 single crystals. (reprinted from ref. 205, Copyright (2008) with permission from the American Chemical Society)

Figure 15 Surface modulation effects induced by surface-selective surfactants on either (reprinted from ref. 58, Copyright (2006) with permission from the John Wiley and Sons) (a) anisotropic nanospindles (reprinted from ref. 216, Copyright (2008) with permission from the John Wiley and Sons) or (b) nanoprisms growth by adsorption with phosphate and oleylamine, respectively. (reprinted from ref. 214, Copyright (2010) with permission from the Royal Society of Chemistry)

Figure 16 TEM micrographs of iron/iron oxide NPs exposed to dry 20% oxygen: (a) <1 min at room temperature; (b) 1 h at 80 °C; (c) 12 h at 80 °C; (d) 1 h at 150 °C; (e) 1 h at 350 °C on a substrate. (reprinted from ref. 97, Copyright (2007) with permission from the American Chemical Society)

Figure 17 Schematic illustration of the morphological evolution process of the iron oxide precursor. (reprinted from ref. 239, Copyright (2006) with permission from the John Wiley and Sons)

Table 1 Typical IONCs with 1D structure by surfactant-assisted hydrothermal method.

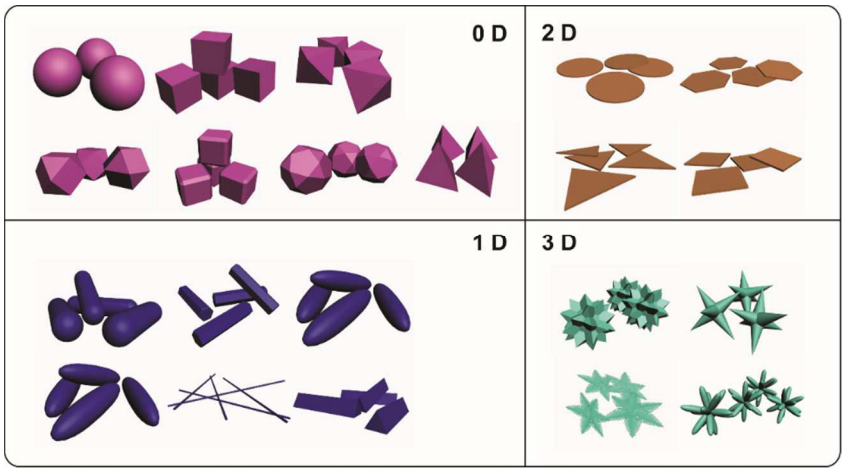

Figure 1

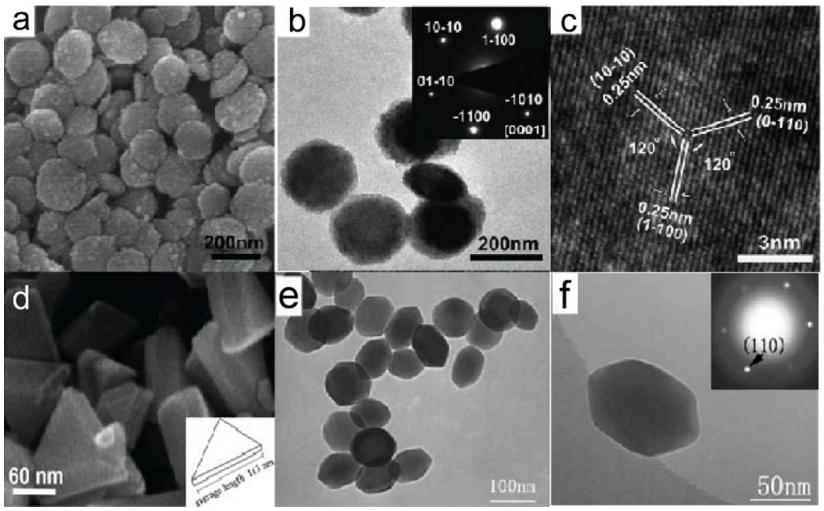

Figure 2

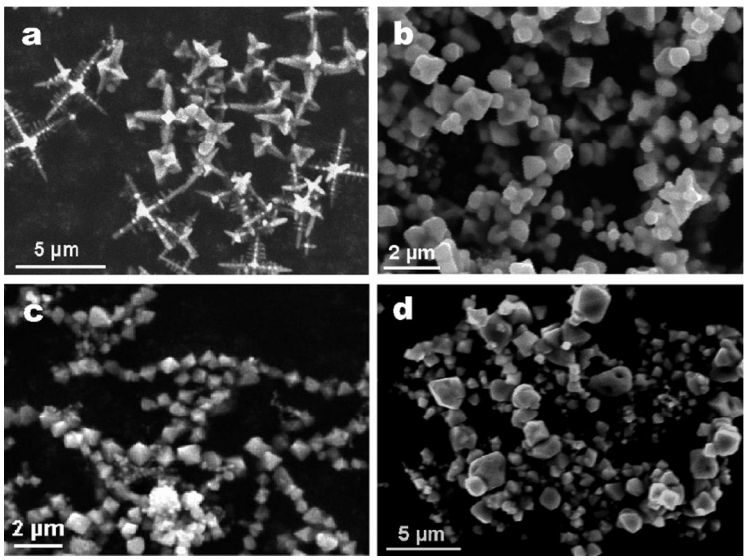

Figure 3

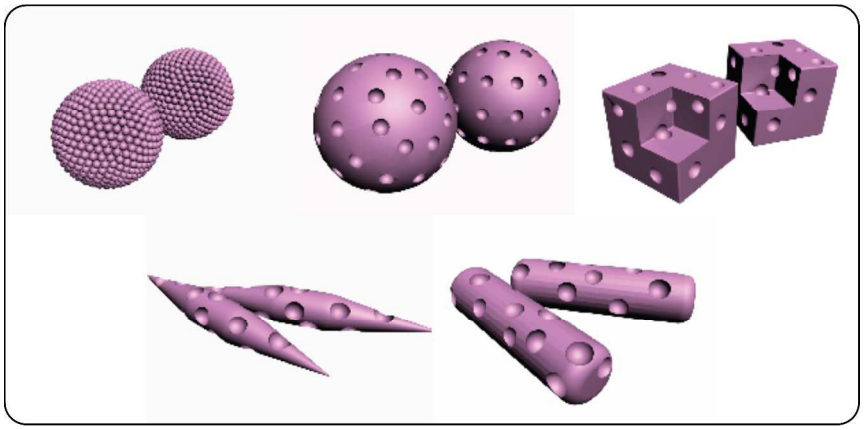

Figure 4

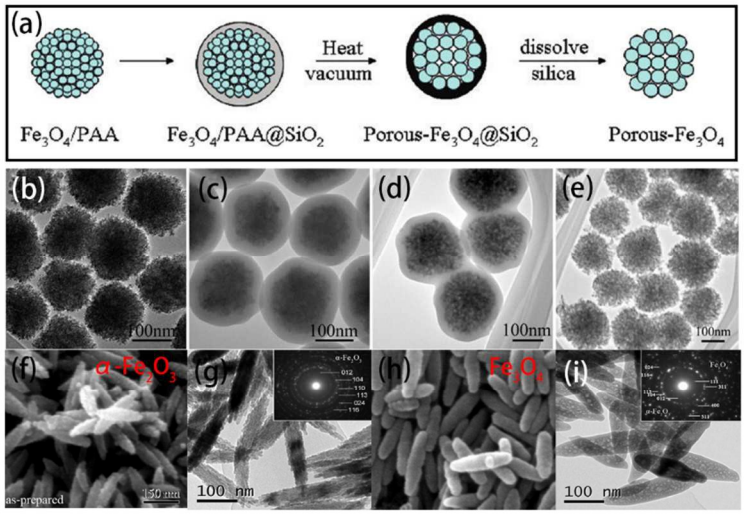

Figure 5

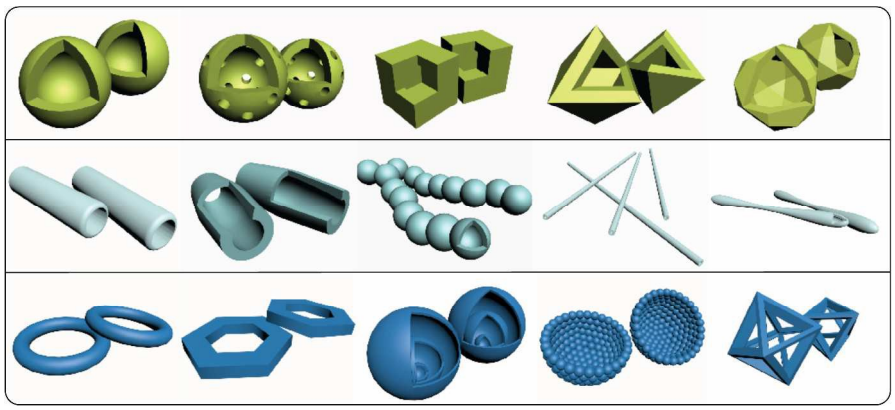

Figure 6

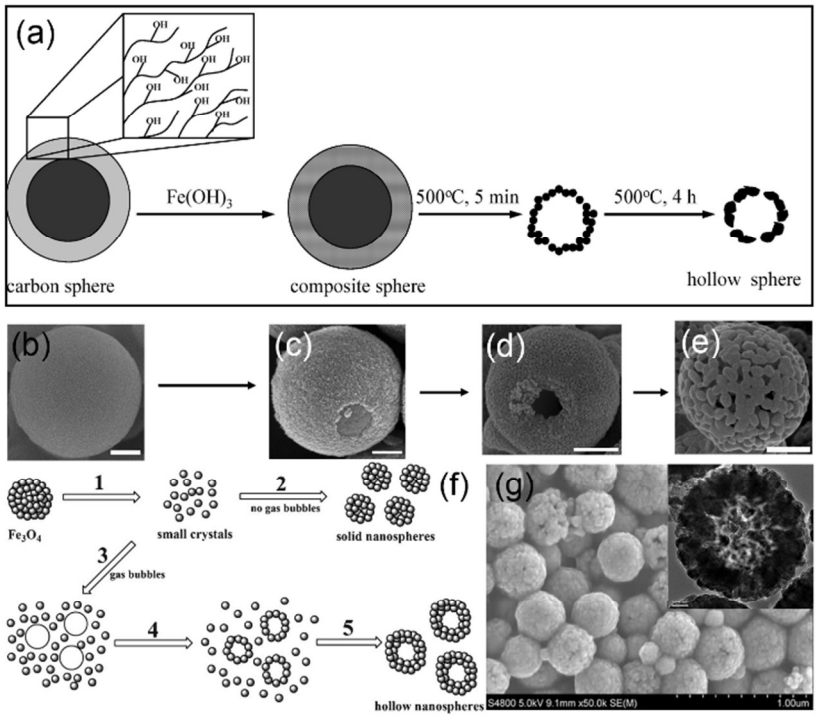

Figure 7

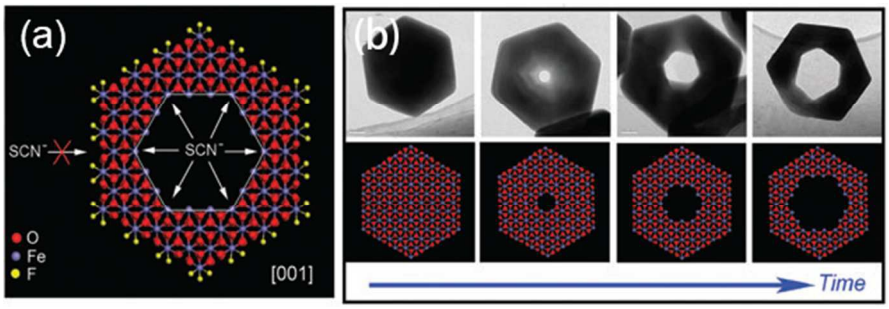

Figure 8

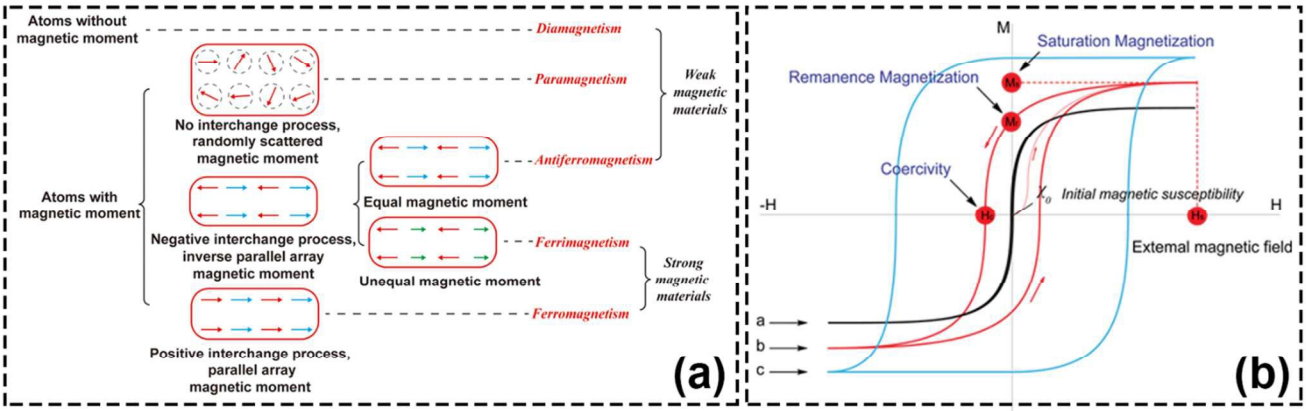

Figure 9

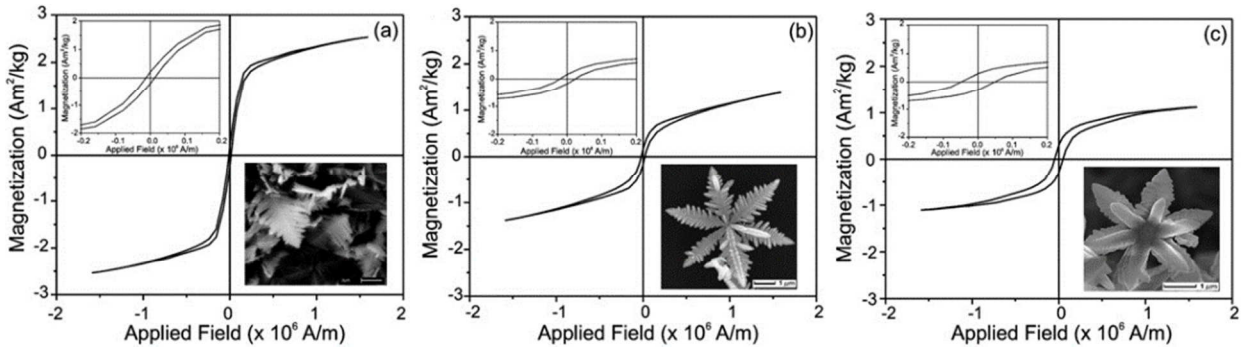

Figure 10

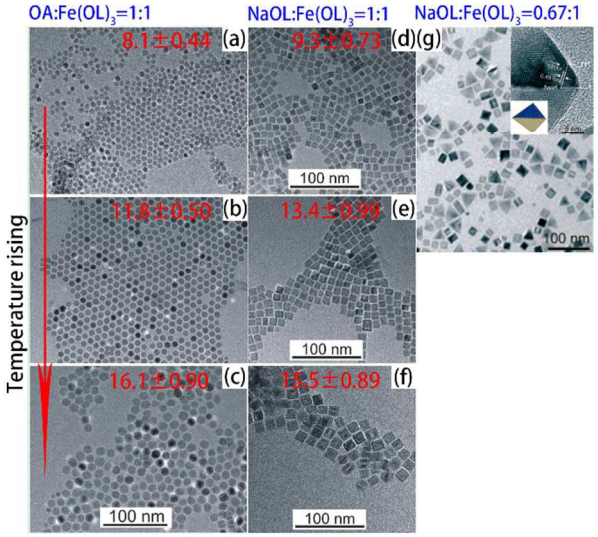

Figure 11

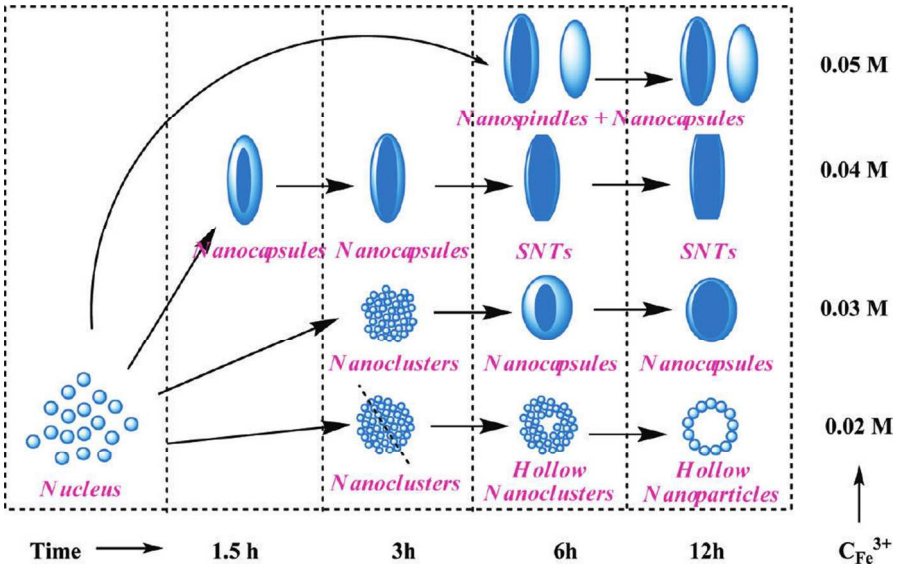

Figure 12

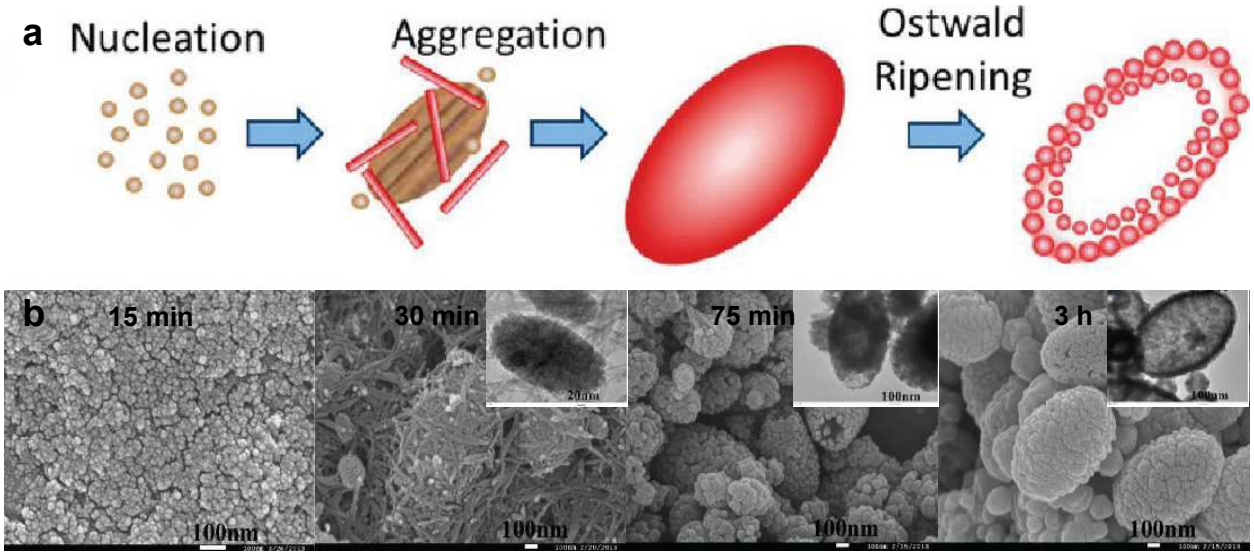

Figure 13

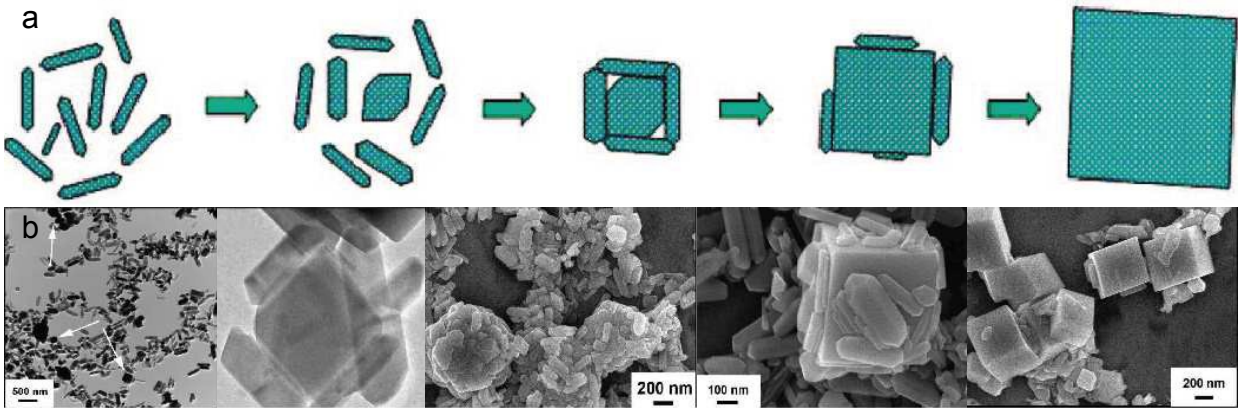

Figure 14

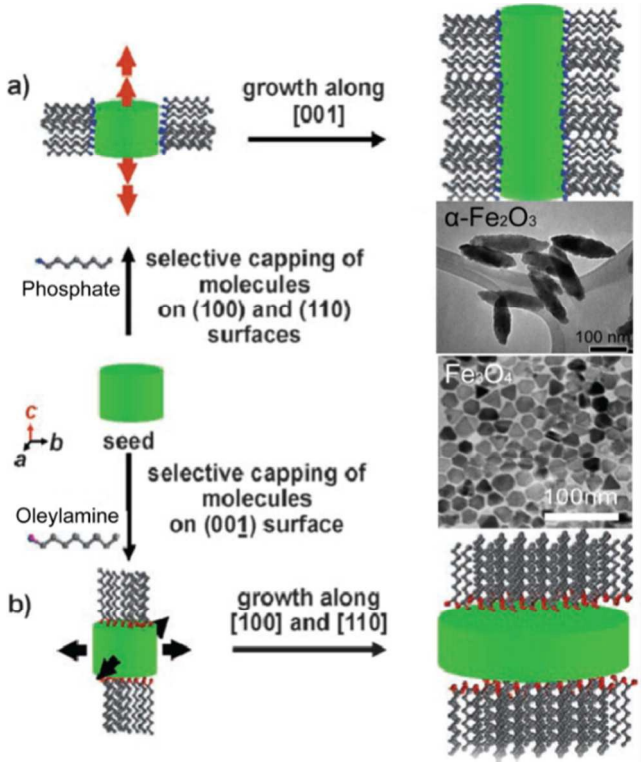

Figure 15

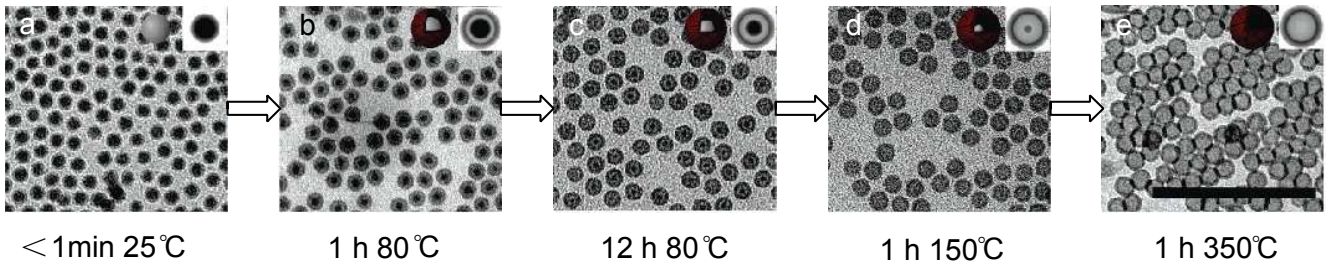

Figure 16

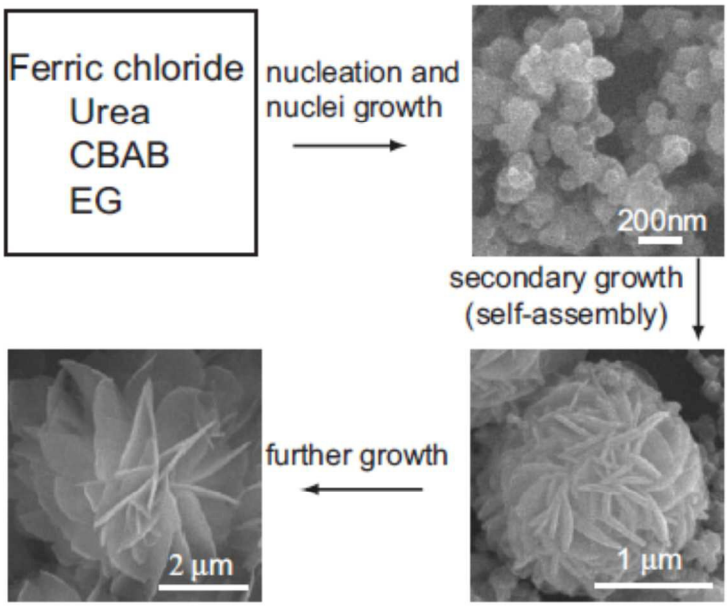

Figure 17